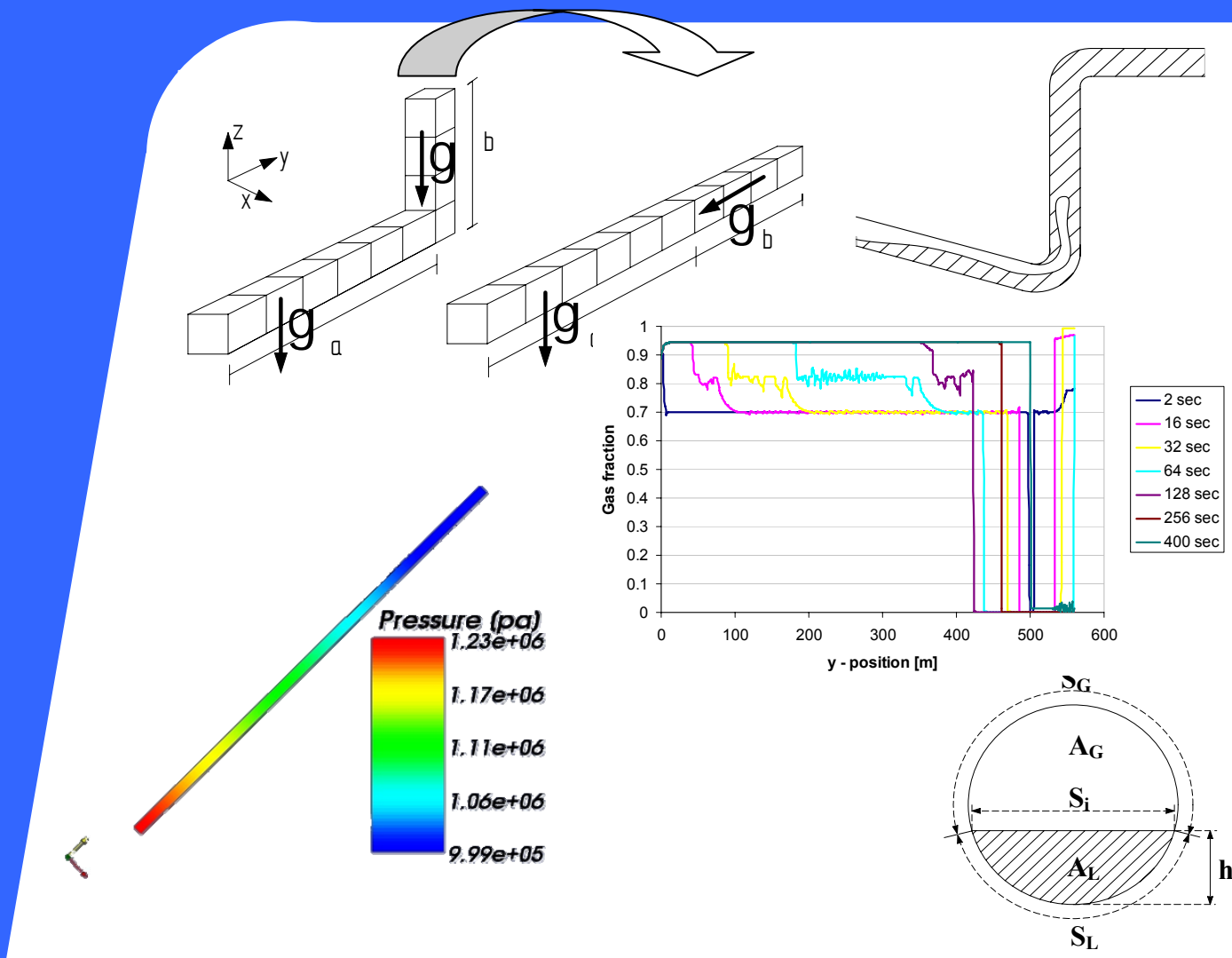


# Development of Transient One-Dimensional Solver for Severe Slugging Simulation



Master Thesis  
 Martin Olldag Bay  
 Oil and Gas Technology  
 Aalborg University Esbjerg  
 2008





# AALBORG UNIVERSITY ESBJERG

**Title:** Development of Transient One- Dimensional  
Solver for Severe Slugging Simulation

**Project period:** May – July, 2008

**Aalborg University Esbjerg**

Niels Bohrs vej 8  
6700 Esbjerg  
Tlf. 79 12 76 66  
Fax 79 12 76 76

**Circulation:** 5

**Pages:** 84

**Enclosed:** CD-ROM

**Supervisors:** Tron Solberg  
Bjørn H. Hjertager

**Front-page:** Selected images from the report

## Preface

This project is the final thesis in the pursuit of the degree Master of Science in Oil and Gas Technology.

The project has been carried out in co-operation with the Process & Loss Prevention Department of Rambøll Oil & Gas, Esbjerg. The project was initially based on a specific practical problem, but as the project progressed the focus was redresses to the development of a transient solver.

This report is addressed to readers with special interest in OpenFOAM, severe slugging phenomenon, or development of new solvers.

I express my gratitude to my supervisors for support and interest. Especially I would like to thank Rolf Hansen, assistant professor, AAUE. I would also direct my gratitude to Asmus D. Nielsen, Director Process & Loss Prevention, Rambøll.

I direct my gratitude to fellow student Claus Hansen for help and support throughout the project.

All OpenFOAM code is presented by the Courier New script.

For referencing and citing the American Chemical Society (ACS) style has been used as described in *The ACS Style Guide*.<sup>1</sup>

---

Martin Olldag Bay

---

<sup>1</sup> Dodd, 1997

---

## Abstract

Severe slugging occurs at pipe-riser systems. The phenomenon is highly undesirable and can have influence on production and damage process equipment. A one-dimensional model is developed in order to simulate the severe slugging phenomenon. The model is developed to the open source program OpenFOAM. The model is tested and all relevant OpenFOAM coding is presented. The model was found capable of capturing physical behavior such as static pressure, friction, and buoyancy. The model is not capable of simulating severe slugging, but future work is proposed in order to achieve this.

## Resumé

‘Severe slugging’ kan forekomme ved rørledning-stiglednings konfigurationer. Fænomenet er uønsket og kan have indflydelse på produktionen og skade proces udstyr. En ét-dimensionel model er udviklet med henblik på at simulere fænomenet. Modellen er udviklet til programmet OpenFOAM. Modellen er testet og alt relevant OpenFOAM kode er præsenteret. Modellen er i stand til at fange fysiske forhold såsom statisk tryk, friktion, og opdrift. Modellen er ikke i stand til at simulere ‘severe slugging’, men kommende arbejde er foreslået for at muliggøre dette.

## Nomenclature

### Roman Letters

$A$	Area	[m <sup>2</sup> ]
$C$	Choke valve coefficient	[-]
$C$	Turbulent/laminar coefficient	[-]
$D$	Diameter	[m]
$F$	Force	[N]
$g$	Acceleration due to gravity	[m/s <sup>2</sup> ]
$h$	Length – riser pipe	[m]
$I$	Indicator function	[-]
$K$	Proportionality constant	[-]
$l$	Length – feed pipe	[m]
$n$	Turbulent/laminar coefficient	[-]
$P$	Pressure	[Pa]
$Q$	Fluid property	[-]
$S_f$	Surface vector	[m <sup>2</sup> ]
$U$	Velocity	[m/s]
$V$	Volume	[m <sup>3</sup> ]
$y$	Introduced disturbance	[m]
$f$	Friction factor	[-]

### Greek Letters

$\alpha$	Gas volumetric fraction	[-]
$\rho$	Density	[kg/m <sup>3</sup> ]
$\sigma$	Stress	[Pa]
$\nu$	Kinematic viscosity	[m <sup>2</sup> /s]
$\Phi$	Void fraction	[-]

## Nomenclature

---

### **Subscripts**

$Q_a$	Phase a
$Q_b$	Phase b
$Q_d$	Diagonal
$Q_f$	Surface
$Q_G$	Gas
$Q_H$	H operator
$Q_L$	Liquid
$Q_N$	Off diagonal matrix
$Q_r$	Relative
$Q_S$	Superficial
$Q_T$	Terminal
$Q_\varphi$	Phase $\varphi$

### **Oversymbols**

$\overline{Q}$	Average
$\tilde{Q}$	Density averaged
$\hat{Q}$	Interface average

## Table of contents

<b>1</b>	<b>INTRODUCTION.....</b>	<b>1</b>
1.1	OBJECTIVE .....	1
1.2	PROJECT STRUCTURE.....	2
<b>2</b>	<b>SEVERE SLUGGING .....</b>	<b>3</b>
2.1	DESCRIPTION OF SLUGGING CYCLE.....	3
2.2	PRODUCTION DURING SLUGGING CYCLE.....	4
2.3	PRESSURE DEVELOPMENT DURING SLUGGING CYCLE .....	5
2.4	STABILITY CRITERION .....	5
2.5	EFFORTS TO PREVENT SLUGGING .....	9
<b>3</b>	<b>BASIC BUILD UP OF SOLVER.....</b>	<b>13</b>
3.1	CONDITIONAL AVERAGING .....	13
3.2	CONDITIONAL AVERAGED TRANSPORT EQUATION .....	15
3.3	EQUATION CLOSURE .....	17
3.4	FINITE VOLUME NOTATION .....	18
3.5	SOLUTION ALGORITHM.....	20
3.6	INITIAL TEST OF SOLVER.....	20
<b>4</b>	<b>FRICTION MODEL.....</b>	<b>25</b>
4.1	MOMENTUM TRANSFER BETWEEN GAS AND PIPE .....	25
4.2	MOMENTUM TRANSFER BETWEEN GAS AND LIQUID.....	28
4.3	MOMENTUM TRANSFER BETWEEN LIQUID AND PIPE .....	28
<b>5</b>	<b>PIPE INCLINATION .....</b>	<b>29</b>
<b>6</b>	<b>REVIEW OF OPENFOAM .....</b>	<b>31</b>
<b>7</b>	<b>OPENFOAM SOLVER.....</b>	<b>32</b>
7.1	1DSLUGFOAM .....	33
7.2	CREATEFIELDS.H.....	34
7.3	ALPHAEQN.H.....	35
7.4	DRAG.H.....	36
7.5	UEQNS.H .....	37
7.6	PEQN.H .....	38
<b>8</b>	<b>CASE STRUCTURE .....</b>	<b>40</b>
8.1	0 – DIRECTORY .....	41
8.2	CONSTANT .....	43
8.3	SYSTEM .....	45
<b>9</b>	<b>SIMULATION OF PIPE-RISER SYSTEM .....</b>	<b>47</b>
9.1	SIMULATING STABLE SYSTEM.....	47
9.2	SIMULATING UNSTABLE SYSTEM .....	54
9.3	SUMMARY OF RESULTS.....	58
<b>10</b>	<b>DISCUSSION .....</b>	<b>59</b>
10.1	REFINEMENT OF FRICTION MODEL .....	59
10.2	IMPLEMENTATION OF COMPRESSIBILITY.....	59
10.3	FUTURE WORK.....	60
<b>11</b>	<b>CONCLUSION.....</b>	<b>61</b>
<b>APPENDIX A</b>	<b>FLOW PATTERNS .....</b>	<b>64</b>



# 1 Introduction

The oil and gas industry has been compelled to focus on marginal fields since the demand for oil is increasing and no new super fields have been discovered recently. This has triggered a revolution in oil production methods and new radical engineering solutions have been implemented in order to reduce the costs and thereby make marginal fields economically viable. One of these solutions has been the transportation of the production fluids. At larger fields it can be justified to separate the fluids prior to transportation and transport it in separate pipelines. At marginal fields it has proven more economically viable to transport in one, which has created a demand for understanding multi-phase transport phenomena.

Initially multi-phase transport was simplified and treated as one homogeneous mixture, with average properties. Rules of thumb were utilized to account for the unstable behaviour of the multi-phase flow. These rules of thumb have proven sufficient at normal operating conditions, but as the production moves to more demanding fields they are no longer applicable. Consequently, a more profound understanding of the multi-phase flow is requested so more comprehensive models for multi-phase flow can be developed.

A critical multi-phase flow challenge is the terrain induced slugging phenomenon. This area is of great importance due to the long-duration instabilities and the related oscillating momentum which can damage process equipment and necessitate major slug catchers. Terrain induced slugging is highly undesirable and several actions be implemented to prevent this type of slugging. Terrain induced slugging at a pipeline-riser system is denoted severe slugging and is often prevented by implementing choke valves. This will, however, affect the production. Alternatively, a gas lift technique can be implemented, but this method is still on an experimental stage.

By understanding the terrain induced slugging the cause and effect can be included in the design phase and unpleasant surprises at the production phase can be avoided. A model capable of simulating the terrain induced slugs could predict, not only if terrain induced slugging would occur, but also important slug flow characteristics such as velocities, slug length, and slug intervals.

For slug modelling, engineers can resort to commercial codes such as OLGAS but the commercial licenses are often expensive. Therefore a relatively high number of multiphase investigations are required in order to justify the expense of the license. Furthermore, these codes rarely offer insight in the calculations for the user, which can lead to poor understanding and thereby crucial errors.

## 1.1 Objective

For the above mentioned reasons it could be advantageous to develop a program, which could predict terrain induced slugging and determine vital flow characteristics.

The program should be developed using an open source to avoid the cost of commercial licenses. It should offer insight in the calculations and provide opportunity to apply features to it, such as a thermodynamic model or effects of process equipment. It is therefore chosen to develop the model in OpenFOAM vers. 1.4.1 (Open Field Operation And Manipulation). OpenFOAM is an opensource C++ toolbox for numerical solvers in

continuum mechanics. OpenFOAM does not only provide a list of basic solvers but it also offers the opportunity to develop new specific solvers.

It is chosen to develop the model in one dimension. The slug cycle time is relatively long compared to a discretised time step, which will cause an unacceptable number of calculations if the interface has to be incorporated in the iterative calculations. By applying a one dimensional solver it is possible to express the interfacial contribution by averaged values. Furthermore, the length of the pipe system is much greater than the pipe diameter and therefore can the system be regarded as one-dimensional.

A one dimensional, transient solver is not among the basic solvers in OpenFOAM and it is therefore chosen to develop and implement a new transient one dimensional solver in OpenFOAM in preparation for simulation of severe slugging.

As it would be too comprehensive to develop a fully functional solver it is chosen to focus on the framework for the solver and validate the one dimensional solver. Future work could then comprise simulation of severe slugging and implementation of process equipment.

## 1.2 Project structure

The general approach in this thesis is to initially describe the severe slugging process using basic, simplified, steady state formulas. A short introduction to OpenFOAM is carried out prior to the description of the theory for the basic build up of the one dimensional solver.

A section explaining the friction model utilized follows and subsequently an analysis of the incorporation of the pipe inclination is carried out. Hereafter the programming structure in OpenFOAM is presented and the case structure representing the physical layout of the pipeline and CFD-technical parameters are accounted for.

Finally, the results of the solver are presented and suggestions for future work on the solver are given.

## 2 Severe slugging

In order to develop a program applicable to capture severe slugging an analysis of the triggering effects must be carried out. It is important to specify the governing effects that take place when slugging occurs in order to implement them in the model. Initially it is important to distinguish between hydrodynamic slugging and terrain induced slugging. Hydrodynamic slugging occurs at certain flow rates due to a stability criterion between the Bernoulli Effect and gravitational effect. This phenomenon and other flow regimes are described in appendix A – Flow Patterns.

Terrain induced slugging refers to the accumulation of liquid in a lower elbow which results in generation of long slugs. Severe slugging refers to a cyclic occurrence due to liquid accumulation at a pipe-riser system. Severe slugging is normally associated with complications because the production facilities can experience difficulties handling the long slugs. The related high momentum of severe slugging can furthermore cause damage to production facilities. The following analysis of the severe slugging phenomenon is categorised into four sections;

- Description of slugging cycle
- Production during slugging cycle
- Pressure development during slugging cycle
- Efforts to prevent slugging

The following sections will form the basis on which the solver is developed and tested.

### 2.1 Description of slugging cycle

The phenomenon will occur at low gas and liquid flow rates and when the feed pipe to the riser has a downward inclination. Severe slugging will cause periods of no gas and liquid production followed by high gas and liquid productions. The phenomenon is illustrated in figure 2.1.

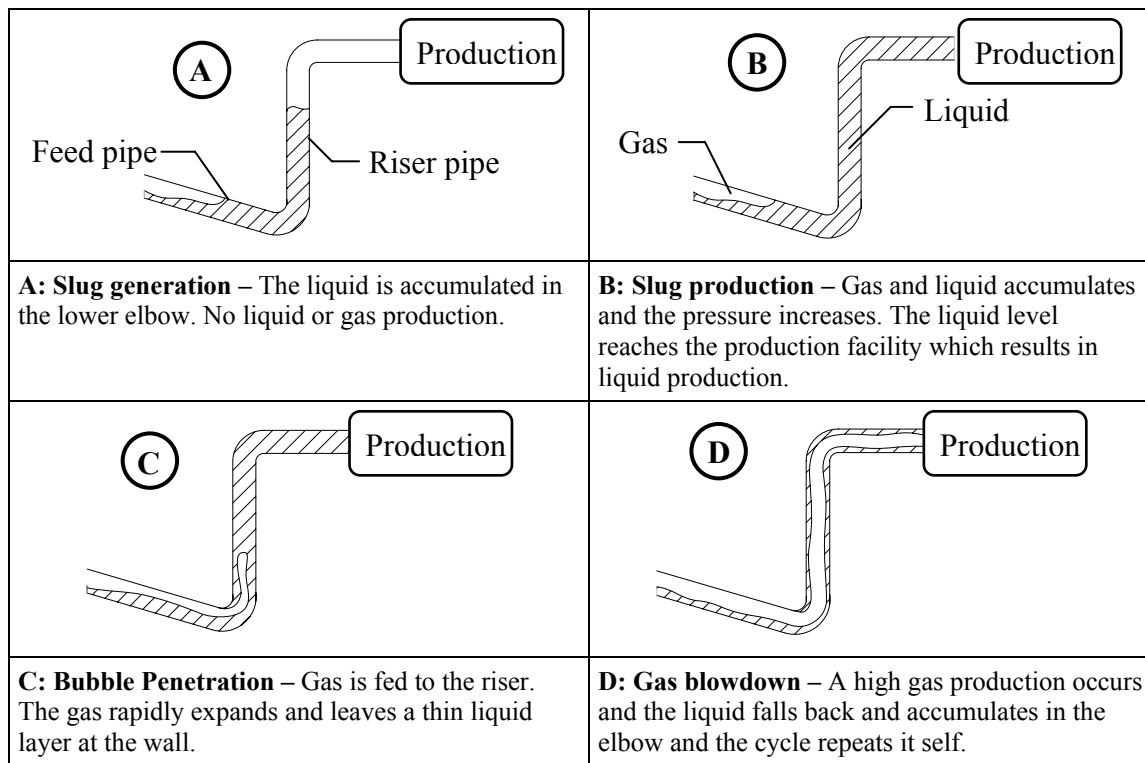


Figure 2.1. The generation of severe slugging.

## 2.2 Production during slugging cycle

The gas and liquid production is depicted in figure 2.2. It is noted that the values of the axis are not of the same dimension and magnitude for liquid production and for gas production. Liquid production is represented as accumulated volume produced and gas production represented as volumetric flow rate. A, B, D, and D refers to slug generation, slug production, bubble penetration, and gas blowdown, respectively. It is noted that bubble penetration occurs in a relatively shorter interval than depicted.

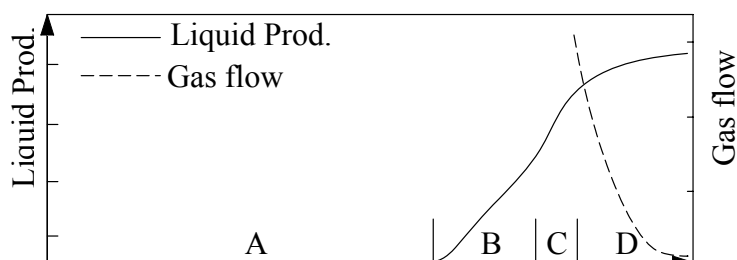


Figure 2.2. Gas and liquid production during a severe slugging cycle.

It is seen from figure 2.2 that liquid production is initiated at the slug production period and the production is stable until bubble penetration occurs. The high velocity gas flow will sustain a liquid production because it will carry small liquid droplets to the riser outlet. The liquid film at the wall will also move upwards initially due to interfacial shear between the phases contributing to additional production. As the pressure drops, the gas

flow rate decreases and the gas velocity becomes insufficient to sustain the existence of a liquid film. The liquid film fall downwards and blocks the pipe before the cycle is repeated.

A rule of thumb frequently used is that the volumetric dimension of the slug is two times the capacity of the riser. This has proven sufficient at moderate riser heights, but the method is not applicable when the height of the riser becomes too great.

## 2.3 Pressure development during slugging cycle

The pressure development during a severe slugging cycle is depicted in figure 2.3. The pressure cycle refers to the pressure at the elbow. A, B, D, and D refers to slug generation, slug production, bubble penetration, and gas blowdown. It is noted that bubble penetration occurs in a relatively shorter interval than depicted.

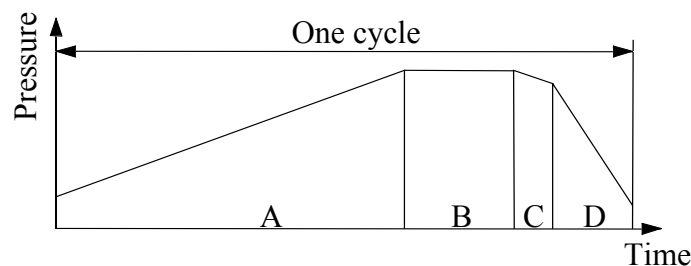


Figure 2.3. Pressure growth during a severe slugging cycle.

It is seen from figure 2.3 that the pressure is rising at the slug generation period. This is due to the change in static head from liquid level build up in the riser pipe. The slug production sets in when the liquid level reaches the riser outlet. The pressure increases only slightly through this phase. As the bubble penetration occurs the pressure relieves because the total density in the riser pipe drops due to the entry of the low-density gas phase.

## 2.4 Stability Criterion

To understand the stability of severe slugging a simplified mathematical model is set up originally considered by Taitel<sup>2</sup>. Here a riser system is considered when the end of the liquid slug reaches the bottom of the riser pipe. This is illustrated in figure 2.4

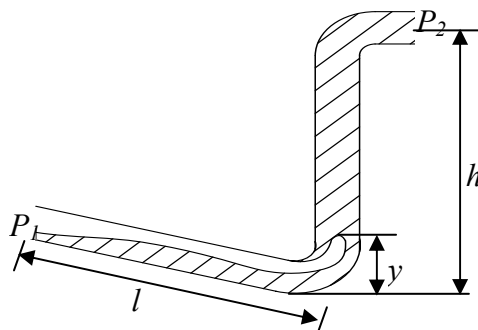


Figure 2.4. Stability of severe slugging.  $h$  refers to the distance between riser outlet and the bottom of the riser.  $y$  refers to an introduced disturbance.

<sup>2</sup> Taitel Y. (1986), "Stability of severe slugging."

Assume a small disturbance introduced to the system depicted as  $y$  at figure 2.4. If friction and acceleration effects are neglected the pressure acting on the interface between the end of the slug and the front of the gas cap yields;

$$\Delta F = \left[ (P_2 + \rho_L \cdot g \cdot h) \frac{\alpha \cdot l}{\alpha \cdot l + \alpha^* \cdot y} \right] - [P_2 + \rho_L \cdot g \cdot (h - y)] \quad (2.1)$$

Where  $\Delta F$ : Net force acting on liquid in riser

$P_2$ : Pressure at riser outlet

$\rho_L$ : Density of liquid

$\alpha$ : Gas hold up in feed pipe

$\alpha^*$ : Gas hold up in the riser

The first term on the right hand side (r.h.s.) corresponds to the driving pressure in the pipeline. The second term refers to the back pressure applied by the liquid column and the riser outlet pressure.

The severe slugging will occur when the driving pressure in the pipeline exceed the back pressure and push gas into the riser thereby causing gas blowdown. This means that blowdown will occur if the net force increases with the disturbance as it is introduced to the riser. this leads to the following statement for stability expressed in equation 2.2;

$$\frac{\partial(\Delta F)}{\partial y} < 0 \quad \text{at} \quad y = 0 \quad (2.2)$$

The net force acting on the interface related to the disturbance level is illustrated in figure 2.5. This is illustrated to clarify the impact different riser heights has on the stability of the system.

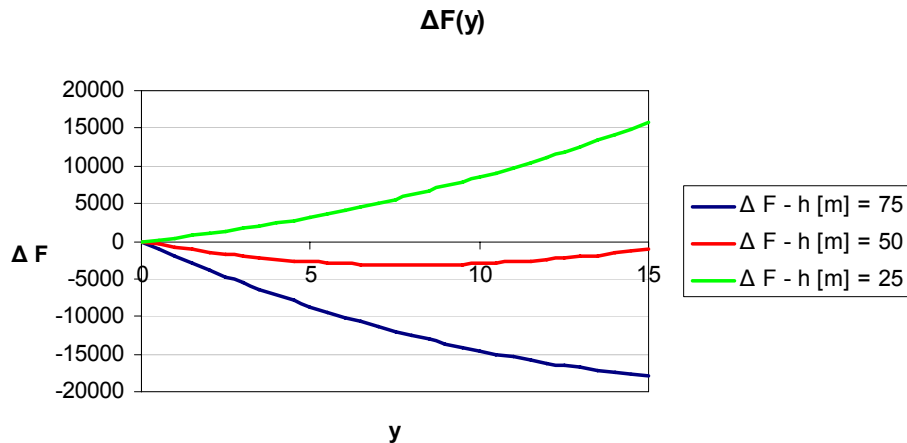


**Figure 2.5. Net force vs. introduced disturbance. The curves represent different riser heights. Separator pressure – 10 bar, liquid density – 800 kg/m<sup>3</sup>, feed pipe length – 150 m, void fraction in riser – 0.7, and void fraction in feed pipe – 0.75.**

It can be seen from figure 2.5 that by increasing the riser length a more stable system is obtained. This is shown by the negative slopes for a riser height of 75 and 50 meters at  $y = 0$ . The positive slope for a riser height of 25 meters indicates an unstable system where severe slugging would occur. The above tendency is due to proportion between the riser

## Severe slugging

height and static pressure which will counteract the driving pressure from the feed pipe and thereby prevent gas blowdown.

In figure 2.6 is net force and disturbance level depicted in order to clarify the impact on stability from riser outlet pressure. The three curves represent different separator pressure.

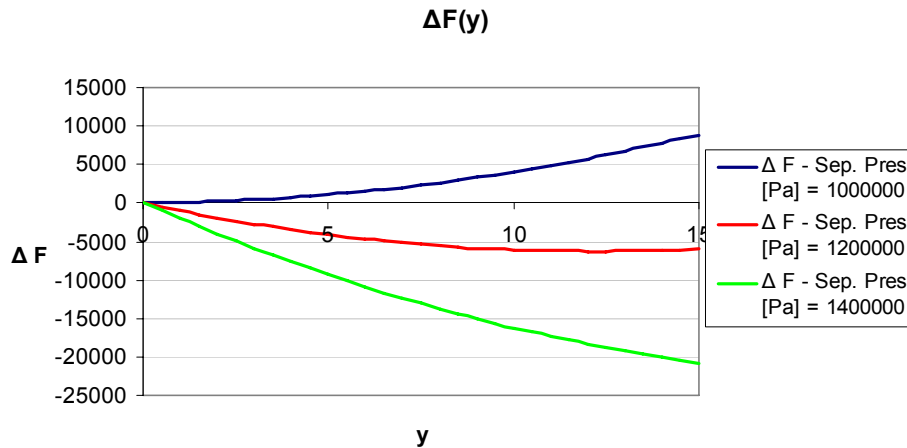


**Figure 2.6. Net force vs. introduced disturbance. The curves represent different separator pressure (riser outlet). Riser height – 60 m, liquid density – 800 kg/m<sup>3</sup>, feed pipe length – 175 m, void fraction in riser – 0.7, and void fraction in feed pipe – 0.75.**

Again a positive slope at  $y=0$  represents an unstable system and a negative slope represents a stable system. It can be seen that by increasing the separator pressure severe slugging can be eliminated and the system will become more stable. The above tendency is because the sum of the separator pressure end static pressure constitutes the counterforce for the feed pipe pressure and thereby increasing the separator pressure will prevent gas blow down.

Figure 2.7 illustrates the impact from feed pipe length. Three different lengths are represented.

As previously stated the driving force is a function of the gas expansion, which is a function of the pipeline gas volume. This volume is represented by a void fraction and a feed pipe length. Figure 2.7 illustrates the impact on stability due to feed pipe length variations. The three curves represent different feed pipe length.

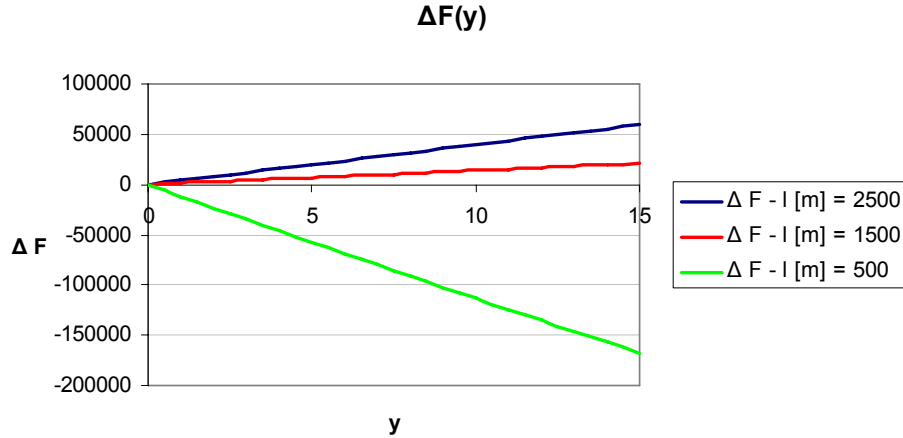


**Figure 2.7. Net force vs. introduced disturbance. The curves represent different feed pipe lengths. Separator pressure – 10 bar, riser height – 60 m, liquid density – 800 kg/m<sup>3</sup>, feed pipe length – 175 m, void fraction in riser – 0.7, and void fraction in feed pipe – 0.75.**

It can be seen from figure 2.7 that an increased feed pipe length introduces instability to the system. As given by the criteria in equation 2.1, the pressure driving force acting on the interface is a function of the gas volume. Increasing the feed pipe length causes a larger gas volume. This is because the driving pressure force is due to the expansion of the gas which will be depending on the gas volume.

A stability criterion can be expressed based on the statement in equation 2.2. It should be noted that the stability criterion neglects friction and acceleration of the fluids. Furthermore are the relatively slow flow rates neglected. The stability criterion therefore yields;

$$\frac{P_2}{P_0} > \frac{\left[ \left( \frac{\alpha}{\alpha^*} \right) \cdot l - h \right] \cdot \rho_L \cdot g}{P_0} \quad (2.3)$$

Where  $P_0$ : Atmospheric pressure

An additional criterion for the stability of the flow is given by the Bøe criterion<sup>3</sup> which is based on a force balance for the blocking liquid slug. The force balance is between the static pressure and the pressure build up in the pipe line. The Bøe criterion is given in equation 2.4.

$$U_{LS} < \frac{P_p}{\rho_L \cdot g \cdot \alpha \cdot l} U_{GS} \quad (2.4)$$

Where:  $P_p$ : Pressure in feed pipe

$U_{LS}$ : Superficial liquid velocity

$U_{GS}$ : Superficial gas velocity

<sup>3</sup> Bøe A. (1981), Severe slugging characteristics.



## 2.5 Efforts to prevent slugging

Initiatives to eliminate severe slugging are to a great extent implemented in the pipe-riser system on account of the unwanted consequences on production and platform facilities caused by severe slugging. Three main techniques are utilized to avoid severe slugging:

- Increased back pressure
- Choking
- Gas lift

The above listed are the three fundamental methods applied. Other methods applied are based on these three fundamental techniques. The governing principle of these three methods will be analysed in the following.

### 2.5.1 Increased back pressure

It can be deduced from equation 2.3 that by increasing  $P_2$  severe slugging can be eliminated. This relates to the method denoted back pressure increase. This is a technique where the separator pressure is raised, here represented as  $P_2$ .

### 2.5.2 Choking

Choking refers to a technique where a valve is implemented to ensure that no gas blow down occurs and thereby securing a stable flow. Choking can be explained by considering the simplified model again, where a choking valve is implemented. The choking valve increases the back pressure in proportion to the velocity in the riser pipe. Consider an unstable system where a control system stabilizes the flow. This system is depicted in 2.8.

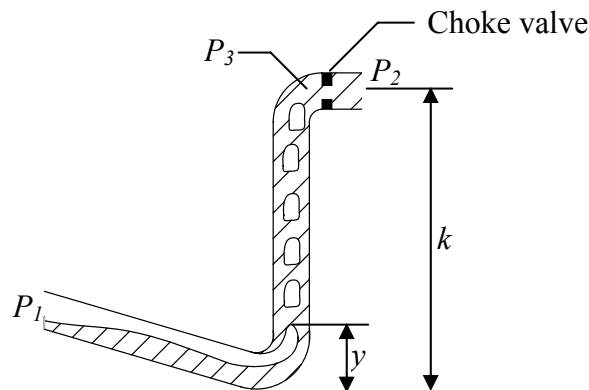


Figure 2.8. Steady unstable system.

The pressure upstream for the choke valve is the sum of the separator pressure and the pressure drop caused by the choking. In addition to this a pressure change occurs as the gas penetrates the riser. When the gas cap enters an instantaneously increase in pressure occurs at the choke valve because the gas pushed the liquid slug. This pressure increase is proportional to the disturbance height  $y$ . The upstream pressure can be expressed as;

$$P_3 = P_2 + C \cdot U_{LS}^2 + K \cdot y \quad (2.5)$$

Where  $C$ : Choke valve coefficient

$K$ : Proportionality constant

Consider the initial stability criterion again.

$$\Delta F = \left[ (P_2 + C \cdot U_{LS}^2 + \rho_L \cdot g \cdot h) \frac{\alpha \cdot l}{\alpha \cdot l + \alpha^* \cdot y} \right] - \left[ P_2 + C \cdot U_{LS}^2 + K \cdot y + \rho_L \cdot g \cdot (h - y) \right] \quad (2.6)$$

By utilizing the stability criterion stated in equation 2.2 and differencing the following stability criterion is obtained;

$$\frac{P_2 + C \cdot U_{LS}^2}{P_0} > \frac{\left[ \frac{\alpha \cdot l}{\alpha^*} \left( 1 - \frac{K}{\rho_L \cdot g} \right) - h \right] \cdot \rho_L \cdot g}{P_0} \quad (2.7)$$

When choking is utilized it is assumed that a steady state operation occurs and thereby the lower elbow is not fully blocked by the liquid. The gas steadily penetrates the riser and the flow regime in the riser pipe appears as either bubble flow or slug flow. (see Appendix A –Flow Patterns). If the gas density is neglected equation 2.7 yields;

$$\frac{P_2 + C \cdot U_{LS}^2}{P_0} > \frac{\left[ \frac{\alpha \cdot l}{\alpha^*} \left( \phi - \frac{K}{\rho_L \cdot g} \right) - \phi \cdot h \right] \cdot \rho_L \cdot g}{P_0} \quad (2.8)$$

As stated earlier the choke coefficient  $C$  and the proportional constant  $K$  direct related. The proportion between the values can be found by assuming the net force balance term in equation 2.6 causes and acceleration of the liquid slug in the riser. This is stated in equation 2.9.

$$A \cdot \Delta F = \frac{d(A(h - y) \cdot \rho_L \cdot U_L)}{dt} \quad (2.9)$$

Where  $A$ : Area of the interface

$U_L$ : Velocity of liquid slug caused by gas penetration

By inserting the expression for the net force in equation 2.7 into equation 2.9 a differential equation for the liquid slug velocity is obtained. This is on account of the statement in equation 2.10.

$$U = \alpha^* \left( \frac{dy}{dt} \right) \quad (2.10)$$

The solution for conditions where the ration between the disturbance level and the riser height are small is given in equation 2.11.

$$U^2 = U_{LS}^2 + \frac{2}{h} \cdot U_{LS}^2 \cdot y \quad (2.11)$$

The pressure drop across the choking valve can be expressed as a function of the liquid slug velocity and therefore:

$$P_3 - P_2 = C \cdot U^2 \quad (2.12)$$

By substituting equation 2.11 into equation 2.12 and inserting equation 2.5 into the generated expression the direct relationship between the choking coefficient and the proportionality coefficient is obtained. The relationship is given in equation 2.13.

$$K = \frac{2 \cdot C \cdot U_{LS}^2}{h} \quad (2.13)$$

### 2.5.3 Gas lift

Gas lift refers to a technique where gas is compressed and injected into the riser pipe. It can be explained by considering the stability criterion where only the injected gas is considered. This is expressed in equation 2.14.

$$\frac{P_2}{P_0} > \frac{\left[ \frac{\alpha \cdot l}{\alpha^*} - h \right] \cdot \Phi_{GL} \cdot \rho_L \cdot g}{P_0} \quad (2.14)$$

Where  $\phi_{GL}$ : Volume fraction of liquid in riser caused by gas lift only

The volume fraction can be determined by equation 2.15

$$\Phi_{GL} = 1 - \frac{U_{GSGL}}{U_T} \quad (2.15)$$

Where  $U_T$ : Terminal velocity

$U_{GSGL}$ : Superficial gas velocity for injected gas

The terminal velocity is calculated by equation 2.16. The terminal velocity is the sum of the drag contribution and an additional velocity due to buoyancy. The terminal velocity is expressed by equation 2.16.

$$U_T = C_0 \cdot U_S + U_0 \quad (2.16)$$

$U_0$  is defined as the velocity of the gas bubbles relative to the average velocity.  $C_0$  is a factor correlating for the fact the liquid velocity at certain flow regimes is greater in areas where the bulk gas flows than the average velocity. The terminal velocity is dependent on the flow regime. The flow regime is described in Appendix A – Flow Patterns and the factors for determining terminal velocity for bubble flow were determined by Nicklin et al<sup>4</sup>.

$$\begin{aligned} C_0 &= 1.2 \\ U_0 &= 0.35 \cdot \sqrt{g \cdot D} \end{aligned} \quad (2.17)$$

The factors for terminal velocity in slug flow were determined by Harmathy<sup>5</sup>.

$$\begin{aligned} C_0 &= 1 \\ U_0 &= 1.53 \cdot \left[ \frac{g \cdot (\rho_L - \rho_G) \cdot \sigma}{\rho_L^2} \right]^{\frac{1}{4}} \end{aligned} \quad (2.18)$$

Where  $D$ : Pipe diameter

---

<sup>4</sup> Nicklin et al. (1962), “The Onset of Instability in Two Phase Slug Flow.”

<sup>5</sup> Harmathy T.Z. (1960), “Velocity of Large Droplets and Bubbles in Media...”

$\sigma$  : Surface tension

The gas in the riser will at steady state operation be constituted by the gas injected and the gas penetrating from the feed pipe. The stability criterion at steady state yields;

$$\frac{P_2}{P_0} > \frac{\left[ \frac{\alpha \cdot l}{\alpha^*} - h \right] \cdot \Phi_T \cdot \rho_L \cdot g}{P_0} \quad (2.19)$$

$\phi_T$  is the total liquid volume fraction in the riser. This variable can be determined by equation 2.20.

$$\Phi_T = 1 - \frac{(U_{GSL} + U_{GS})}{U_T} \quad (2.20)$$

The superficial velocity is the sum of the superficial liquid velocity, superficial gas velocity from the gas lift application, and the superficial gas velocity due to the gas flow rate.

### 3 Basic build up of solver

This section will describe the basic build up of the solver. It will go through the theory on which the solver is based on. The discretion of the basic terms will be clarified and the discretised closure models are presented.

The one dimensional form for the model is obtained by averaging flow properties over the cross sectional area of the pipe. Momentum transfer between the fluids and between the pipe wall and the fluids are incorporated by equations expressed as the source term. A two phase algorithm using conditional averaging with discretised terms have been developed by Weller<sup>6</sup>. However, this was done for non-averaged flow properties and therefore a new deduction of the two-phase algorithm is performed. This section is subdivided into the following;

- Conditional averaging
- Conditional averaged transport equations
- Equation closure
- Finite Volume Notation
- Solution algorithm
- Initial test of solver

The following sections will present the one dimensional model on which the solver is based on.

#### 3.1 Conditional averaging

Averaging is used to separate and decompose a fluid property into sub-elements, e.g. phases. Dopazo<sup>7</sup> suggested that instead of Reynolds averaging it could advantageous to apply a conditional averaging technique. Weller<sup>8</sup> applied the technique to multiphase flow. He considered the phases separated by an infinitely thin interface and applied an indicator function for conditional averaging.

Consider the indicator function expressed as;

$$I_{\varphi}(x,t) = \begin{cases} 1 & \text{if } (x,t) \text{ is in phase } \varphi \\ 0 & \text{otherwise} \end{cases} \quad (3.1)$$

Then the volume phase fraction  $\alpha_{\varphi}$  is defined as the probability of being in phase  $\varphi$  at position  $(x,t)$ ;

$$\alpha_{\varphi} = \overline{I_{\varphi}}(x,t) \quad (3.2)$$

The conditional average of fluid property  $Q$  can be defined as;

$$\overline{I_{\varphi} Q} = \alpha_{\varphi} \overline{Q_{\varphi}} \quad (3.3)$$

<sup>6</sup> Weller H.G. (2005), "Derivation, Modelling and Solution of the Conditionally Averaged Two-Phase..."

<sup>7</sup> Dopazo C. (1977), "On Conditional Averages for Intermittent turbulent flows"

<sup>8</sup> Weller H.G. (1993), "The Development of a New Flame Area Combustion Model Using conditional..."

Similarly, the phase mass fraction equivalent to the density weighted volume fraction be defined as;

$$\widetilde{\rho\alpha_\varphi} = \overline{\rho_\varphi\alpha_\varphi} \quad (3.4)$$

Hence the density weighted conditional average of fluid property  $Q$  is expressed as;

$$\overline{I_\varphi\rho Q} = \alpha_\varphi \overline{\rho_\varphi\widetilde{Q}_\varphi} \quad (3.5)$$

Standard approach is then to decompose the instantaneous fluid property into an average contribution and a fluctuating contribution. A one-dimensional can neglect the fluctuating contribution and thereby the method significantly simplified.

The differential operation of the indicator function can be written as

$$\begin{aligned} \overline{\nabla I_\varphi Q} &= \nabla(\overline{I_\varphi Q}) = \nabla(\alpha_\varphi \overline{Q}_\varphi) \\ \frac{\partial \overline{I_\varphi Q}}{\partial t} &= \frac{\partial(\overline{I_\varphi Q})}{\partial t} = \frac{\partial(\alpha_\varphi \overline{Q}_\varphi)}{\partial t} \end{aligned} \quad (3.6)$$

Consider the derivative of the product of the fluid property and the identity function. By the product rule this is given by;

$$\nabla(I_\varphi Q) = I_\varphi(\nabla Q) + (\nabla I_\varphi)Q$$

The mean of  $I_\varphi(\nabla Q)$  over control volume  $\delta V$  can then be expressed as;

$$\overline{I_\varphi \nabla Q} = \nabla(\overline{I_\varphi Q}) - \lim_{\delta V \rightarrow 0} \frac{1}{\delta V} \int_{S(x,t)} n_\varphi Q(x,t) dS \quad (3.7)$$

Equation 3.7 takes this form because  $\nabla I_\varphi$  is only non-zero at the interface described by  $S(x,t) = 0$ . The magnitude of  $\nabla I_\varphi$  at this location is the value of the Dirac delta function and with direction of the unit vector  $n_\varphi$  normal to the interface pointing into phase  $\varphi$ .

The interface average  $\widehat{Q}$  of fluid property  $Q$  is defined as the surface integral per control volume divided by the surface area per control volume.

$$\widehat{Q} = \frac{\lim_{\delta V \rightarrow 0} \frac{1}{\delta V} \int_{S(x,t)} Q(x,t) ds}{\Sigma} \quad (3.8)$$

Where  $\Sigma$  : Surface area per control volume

So equation 3.7 can be expressed by equation 3.8 and 3.6;

$$\overline{I_\varphi \nabla Q} = \nabla(\alpha_\varphi \overline{Q}_\varphi) - \widehat{n_\varphi Q} \Sigma \quad (3.9)$$

Applying same method as for the deduction of equation 3.9 it can be shown that;

$$\overline{I_\varphi \nabla \cdot Q} = \nabla \cdot (\alpha_\varphi \overline{Q}_\varphi) - \widehat{n_\varphi \cdot Q} \Sigma \quad (3.10)$$

And that;

$$\overline{I_\varphi \frac{\partial Q}{\partial t}} = \frac{\partial \alpha_\varphi \overline{Q}_\varphi}{\partial t} + \widehat{Q n_\varphi \cdot U_s} \Sigma \quad (3.11)$$

Where  $U_s$ : Velocity of interface

## 3.2 Conditional averaged transport equation

It is necessary to perform the above describe conditional averaging to the transport equations, because of the multi phase circumstances. Conditionally averaging is applied to the transport equations by multiplying with the indicator function. The transport equations are constituted from;

- Continuity equation
- Momentum equation

### 3.2.1 Continuity equation

Consider the continuity equation given by equation 3.12.

$$\frac{\partial \rho}{\partial t} + \nabla \cdot (\rho U) = 0 \quad (3.12)$$

Multiplying with the indicator function and utilizing equation 3.10 and 3.11 to simplify equation 3.12 now yields;

$$\frac{\partial \alpha_\varphi \overline{\rho}_\varphi}{\partial t} + \widehat{\rho n_\varphi \cdot U_s} \Sigma + \nabla \cdot (\alpha_\varphi \overline{\rho}_\varphi U_\varphi) - \widehat{\rho n_\varphi \cdot U} \Sigma = 0 \quad (3.13)$$

Combining the contributions from the surface average and utilizing density weighted conditional averaging to the expression for  $\rho$  and  $U$  gives;

$$\frac{\partial \alpha_\varphi \overline{\rho}_\varphi}{\partial t} + \nabla \cdot (\alpha_\varphi \overline{\rho}_\varphi \widetilde{U}_\varphi) = \widehat{\rho n_\varphi \cdot (U - U_s)} \Sigma \quad (3.14)$$

At the interface the difference between the fluid velocity and the inter face velocity is given by the mass transfer rate between the phases. This can be expressed by the interface propagation speed  $S_\varphi$  and the interface normal  $n_\varphi$ . Hence, can equation 3.14 be simplified and yields.

$$\frac{\partial \alpha_\varphi \overline{\rho}_\varphi}{\partial t} + \nabla \cdot (\alpha_\varphi \overline{\rho}_\varphi \widetilde{U}_\varphi) = -\widehat{\rho_\varphi S_\varphi} \Sigma \quad (3.15)$$

Equation 3.15 is the final form of the continuity equation. It does, however, need further boundedness and discretisation.

### 3.2.2 Momentum equation

Consider the momentum equation given by equation 3.16.

$$\frac{\partial \rho U}{\partial t} + \nabla \cdot (\rho U U) = -\nabla \cdot \sigma + \rho g \quad (3.16)$$

The total stress term can be decomposed into an isotropic static pressure part and a deviatoric part. Due to the one-dimensionality of the model the latter are left out. Again,

conditional averaging is applied by multiplying with the indicator function and utilizing the previous derived conditional averaging operation.

$$\begin{aligned} \frac{\partial \alpha_\phi \overline{\rho_\phi} \widetilde{U}_\phi}{\partial t} + \widehat{\rho U n_\phi \cdot U_s} \Sigma + \nabla \cdot (\alpha_\phi \overline{\rho_\phi} \widetilde{U}_\phi \widetilde{U}_\phi) - \widehat{\rho U n_\phi \cdot U} \Sigma = \\ -\nabla (\alpha_\phi \overline{p_\phi}) + \widehat{n_\phi p} \Sigma + \alpha_\phi \overline{\rho_\phi} g \end{aligned} \quad (3.17)$$

Equation 3.17 can be simplified by rearranging the interface average terms.

$$\begin{aligned} \frac{\partial \alpha_\phi \overline{\rho_\phi} \widetilde{U}_\phi}{\partial t} + \nabla \cdot (\alpha_\phi \overline{\rho_\phi} \widetilde{U}_\phi \widetilde{U}_\phi) + \widehat{\rho U S_\phi} \Sigma = \\ -\nabla (\alpha_\phi \overline{p_\phi}) + \widehat{n_\phi p} \Sigma + \alpha_\phi \overline{\rho_\phi} g \end{aligned} \quad (3.18)$$

The interface averaged correlation term can be decomposed into an average contribution and a surface fluctuating contribution. The average contribution from the interface can be related to the in-phase average and hence equation 3.18 now yields;

$$\begin{aligned} \frac{\partial \alpha_\phi \overline{\rho_\phi} \widetilde{U}_\phi}{\partial t} + \nabla \cdot (\alpha_\phi \overline{\rho_\phi} \widetilde{U}_\phi \widetilde{U}_\phi) = -\alpha_\phi \nabla \overline{p_\phi} + \alpha_\phi \overline{\rho_\phi} g \\ + \widehat{\rho U S_\phi} \Sigma + (\widehat{p} - \overline{p_\phi}) \nabla \alpha_\phi + \widehat{n_\phi p^\#} \Sigma - \widehat{\rho U S_\phi} \Sigma + \end{aligned} \quad (3.19)$$

An interface momentum transfer between the phases must be modeled with respect to  $M_c = -M_d$ . This can be secured by expressing the interface momentum transfer by equation 3.20.

$$M_\phi = (\widehat{p} - \langle p \rangle) \nabla \alpha_\phi + \widehat{n_\phi p^\#} \Sigma \quad (3.20)$$

Where  $\langle p \rangle$ : Pressure function of conditional average for both phases.

By inserting the momentum transfer expression in equation 3.20 into equation 3.19 the conditional averaged momentum equation yields;

$$\begin{aligned} \frac{\partial \alpha_\phi \overline{\rho_\phi} \widetilde{U}_\phi}{\partial t} + \nabla \cdot (\alpha_\phi \overline{\rho_\phi} \widetilde{U}_\phi \widetilde{U}_\phi) = -\alpha_\phi \nabla \overline{p_\phi} + \alpha_\phi \overline{\rho_\phi} g \\ - \widehat{\rho U S_\phi} \Sigma + M_\phi + (\widehat{p} - \overline{p_\phi}) \nabla \alpha_\phi - (\widehat{p} - \langle p \rangle) \nabla \alpha_\phi \end{aligned} \quad (3.21)$$

Equation 3.21 is the final form of the momentum equation. It does, however, require further modeling of the interface momentum transfer rate, surface mass transfer and an averaging procedure to obtain the pressure function of conditional averaging for both phases.

It is obvious that equation 3.21 needs an expression for the momentum transfer due to friction between the fluids and the wall in addition to the interface momentum transfer. As previously stated this will be implemented by a source term based on empirical correlations. However, to maintain simplicity these expressions are outlined in Section 4 Friction model. For now the friction contribution will be expressed simplified as  $F_{fric}$  and equation 3.21 yields;



$$\begin{aligned} \frac{\partial \alpha_\phi \overline{\rho_\phi} \widetilde{U}_\phi}{\partial t} + \nabla \cdot (\alpha_\phi \overline{\rho_\phi} \widetilde{U}_\phi \widetilde{U}_\phi) = & -\alpha_\phi \nabla \overline{p_\phi} + \alpha_\phi \overline{\rho_\phi} g \\ -\overline{\rho U S_\phi} \Sigma + M_\phi + (\widehat{p} - \overline{p_\phi}) \nabla \alpha_\phi - (\widehat{p} - \langle p \rangle) \nabla \alpha_\phi + F_{fric} \end{aligned} \quad (3.22)$$

### 3.3 Equation closure

Consider the continuity equation. Initially it is assumed that the flow is incompressible and the density weighted expression can therefore be simplified to only account for the un-weighted term. Equation 3.15 can therefore be written as;

$$\frac{\partial \alpha_\phi}{\partial t} + \nabla \cdot (\overline{U}_\phi \alpha_\phi) = 0 \quad (3.23)$$

It is crucial to obtain boundedness of the continuity equation. Applying a limited discretisation scheme would only secure boundedness in one extreme of the volume fraction end. An option to ensure boundedness is to decompose the fraction velocity into a mean and relative part. This is expressed in equation

$$\overline{U}_a = \overline{U} + \alpha_b \overline{U}_r$$

Where  $\overline{U}$  : Mean velocity. Defined as  $\overline{U} = \alpha_a \overline{U}_a + \alpha_b \overline{U}_b$

$\overline{U}_r$  : Relative velocity between the phases. Defined as  $\overline{U}_r = \overline{U}_a - \overline{U}_b$

The continuity equation now yields;

$$\frac{\partial \alpha_a}{\partial t} + \nabla \cdot (\overline{U} \alpha_\phi) + \nabla \cdot (\overline{U}_r \alpha_\phi (1 - \alpha_\phi)) = 0 \quad (3.24)$$

The second term secure boundedness because  $\nabla \cdot (\overline{U} \alpha_\phi) = \nabla \cdot (\overline{U} \cdot \nabla \alpha_\phi)$ , which is an amplitude preserving wave transport term, due to the incompressibility. The second term bounds because it approaches zero as the fraction approaches zero or one. Due to the fact that the second term is non-linear an iterative procedure is required. This iterative procedure can be accelerated by the correction term given in equation 3.25.

$$\alpha_a = \frac{1 - (1 - \alpha_a)^2 + (1 - \alpha_b)^2}{2} \quad (3.25)$$

Now, consider the momentum equation. By assuming that the pressure equals in the phases and that the interface contribution is neglected the momentum equation yields;

$$\frac{\partial \alpha_\phi \overline{\rho_\phi} \widetilde{U}_\phi}{\partial t} + \nabla \cdot (\alpha_\phi \overline{\rho_\phi} \widetilde{U}_\phi \widetilde{U}_\phi) = -\alpha_\phi \nabla \overline{p_\phi} + \alpha_\phi \overline{\rho_\phi} g + M_\phi + F_{fric} \quad (3.26)$$

Difficulties occur when the phase fraction approaches zero. This can be avoided by removing the volume fraction from equation. This is done by dividing by  $\alpha_\phi \rho_\phi$ . The

reason for also dividing with the density is to avoid numerical noise<sup>9</sup>. The momentum equation now yields;

$$\frac{\partial \widetilde{U}_\varphi}{\partial t} + \widetilde{U}_\varphi \cdot \nabla \widetilde{U}_\varphi = -\frac{\nabla \bar{p}}{\rho_\varphi} + g + \frac{M_\varphi}{\alpha_\varphi \rho_\varphi} + \frac{F_{fric}}{\alpha_\varphi \rho_\varphi} \quad (3.27)$$

The interface momentum transfer term and friction term contain the phase fraction. This will be accounted for in section 4 Friction model. It is noted that the momentum equation now expresses acceleration rather than force.

## 3.4 Finite volume notation

Finite volume notation is performed to transform the governing closure equations into a series of algebraic equations by a discretisation scheme.

### 3.4.1 Continuity equation

Initially consider the closure equation of the continuity equation given by equation 3.23. The finite volume version of the continuity equation for phase a is given by equation 3.28;

$$\left[ \frac{\partial [\alpha_a]}{\partial t} \right] + \left[ \nabla \cdot (\phi [\alpha_a]_{f(\phi, scheme)}) \right] + \left[ \nabla \cdot (\phi_{ra} [\alpha_a]_{f(\phi_{ra}, scheme)}) \right] = 0 \quad (3.28)$$

Where  $\phi_{ra}$  : Phase relative flux  $\phi_{ra} = \alpha_{bf(-\phi_r, scheme)} \phi_r$

$\phi_r$  : Relative flux. Defined as  $\phi_r = \phi_a - \phi_b$

The scheme expression subscript denotes that an appropriate scheme has to be used. The f expression in the subscript refers to the value at the cell faces.

### 3.4.2 Momentum equation

The finite volume version of the momentum equation in 3.27 is given in equation 3.29.

$$\begin{aligned} \left[ \frac{\partial [U_a]}{\partial t} \right] + \left[ \nabla \cdot (\phi_a [U_a]) \right] &= -\frac{\nabla \bar{p}}{\rho_a} + g + \frac{M_a}{\alpha_a \rho_a} + \frac{F_{fric-a}}{\alpha_a \rho_a} \\ \left[ \frac{\partial [U_b]}{\partial t} \right] + \left[ \nabla \cdot (\phi_b [U_b]) \right] &= -\frac{\nabla \bar{p}}{\rho_b} + g + \frac{M_b}{\alpha_b \rho_b} + \frac{F_{fric-b}}{\alpha_b \rho_b} \end{aligned} \quad (3.29)$$

There will be accounted for the latter two terms in the equation above in section 4 Friction model. The pressure term on the r.h.s. requires special treatment in order to prevent pressure-velocity decoupling and oscillations. This is done by splitting the momentum equation up and constructing a pressure equation including both the pressure gradient and the gravity term. Hence the momentum equation yields

<sup>9</sup> Crowe C.T. et al. (1994), "Numerical Methods in Multiphase flow"

$$\begin{aligned} \left[ \frac{\partial [U_a]}{\partial t} \right] + \left[ \nabla \cdot (\phi_a [U_a]) \right] &= \frac{M_a}{\alpha_a \rho_a} + \frac{F_{fric-a}}{\alpha_a \rho_a} \\ \left[ \frac{\partial [U_b]}{\partial t} \right] + \left[ \nabla \cdot (\phi_b [U_b]) \right] &= \frac{M_b}{\alpha_b \rho_b} + \frac{F_{fric-b}}{\alpha_b \rho_b} \end{aligned} \quad (3.30)$$

Where:  $M_a = -M_b$

### 3.4.3 Momentum corrector equation

As the term for the pressure gradient is expressed in a separate pressure equation the momentum matrices must be stored without the pressure term.

The phase momentum equation corrector is a term included to account for the pressure gradient, which was excluded from the discretised momentum equation as stated above.

$$\begin{aligned} [M_a [U_a]] &= -\frac{\nabla \bar{p}}{\rho_a} \\ [M_b [U_b]] &= -\frac{\nabla \bar{p}}{\rho_b} \end{aligned} \quad (3.31)$$

The matrix in equation can be decomposed into a diagonal term,  $(M_\phi)_d$  and an H term which is defined as;

$$(M_\phi)_H = (M_\phi)_S - (M_\phi)_N \phi \quad (3.32)$$

Where  $(M_\phi)_S$ : Source vector

$(M_\phi)_N$ : Off diagonal matrix

Because  $\bar{U}_\phi = (M_\phi)_H^{-1} (M_\phi)_D$  the momentum correction term can be stated as

$$\bar{U}_\phi = \frac{(M_\phi)_H}{(M_\phi)_D} - \frac{\nabla \bar{p}}{(M_\phi)_D} \quad (3.33)$$

### 3.4.4 Pressure equation

The pressure equation is based on a volumetric mixture continuity equation, which initially given as

$$\nabla \cdot (\phi) = 0 \quad (3.34)$$

The total face volumetric flux can therefore be written as

$$\nabla \cdot (\alpha_{af} \phi_a + \alpha_{bf} \phi_b) = 0 \quad (3.35)$$

The face volumetric fluxes are based on the momentum corrector term, which easily can be rewritten using central differencing into;

$$\phi_\phi = \phi_\phi^* - \left( \frac{1}{\rho_\phi (M_\phi)_D} \right)_f S_f \nabla_f^\perp \bar{p} \quad (3.36)$$

Where  $\phi_\phi^*$ : Predicted face flux given as  $\phi_\phi^* = \left( (M_\phi)_D^{-1} (M_\phi)_H \right)_f \cdot S_f$

The pressure equation is constructed by substituting equation 3.36 into equation 3.35. The discretised version of the pressure equation therefore yields;

$$\left\| \nabla \cdot \left( \alpha_{af} \left( \frac{1}{\rho_a (M_a)_D} \right)_f + \alpha_{bf} \left( \frac{1}{\rho_b (M_b)_D} \right)_f \right) \nabla \bar{p} \right\| = \nabla \cdot (\alpha_{af} \phi_a^* + \alpha_{bf} \phi_b^*) \quad (3.37)$$

### 3.5 Solution algorithm

The two-fluid solution algorithm is loosely based on a Pressure Implicit with Splitting of Operators (PISO) algorithm, on Weller methodology<sup>6</sup>, and on the existing bubbleFoam solver. It is chosen to rewrite the bubbleFoam solver to adapt it to the one dimension slugging phenomenon in order to avoid errors due to wrongly programmed references in C++. The steps in the algorithm are listed below;

1. Solve alpha equation (3.28)
2. Calculate beta volume fraction
3. Calculate fluid-fluid and fluid-wall momentum transfer rate
4. Solve momentum equation (3.30)
5. Initiate PISO loop
  - a. Predict fluxes by the term representing predicted fluxes in equation (3.36)
  - b. Solve pressure equation (3.37)
  - c. Correct fluxes (3.36)
  - d. Correct velocity (3.33)

### 3.6 Initial test of solver

Initial testing is done here to ensure physical behaviour such as buoyancy effect and friction is properly incorporated into the model. It would be unacceptable if the basic model is unable to capture and simulate basic physic behaviour and the model can therefore be rejected before additional elements are incorporated into the solver. The model will be tested for the following physical conditions:

- Buoyancy effect
- Static pressure
- Friction impact

#### 3.6.1 Buoyancy effect

As one of the phases are lighter than the other it should place it self in the upper part of an inclined pipe. It is tested by letting the mixture of the two fluids flow at low velocity

through an inclined pipe. The densities for the gas and the fluid are  $10 \text{ kg/m}^3$  and  $800 \text{ kg/m}^3$ , respectively. Additional boundary conditions are given in table 3.1.

**Table 3.1. Boundary and initial conditions.**

	$\alpha$	$U_a$	$U_b$	$p$
<b>Internal value</b>	0.4 [-]	0.5 [m/s]	0.5 [m/s]	10e06 [Pa]
<b>Inlet</b>	0.4 [-]	0.5 [m/s]	0.5 [m/s]	zeroGradient
<b>Outlet</b>	zeroGradient	zeroGradient	zeroGradient	10e06 [Pa]

The boundary condition zeroGradient will be further explained in section 8 Case structure. Friction between the pipe wall and fluid are implemented as a function of a constant and a quadrant velocity. One may argue that this term for the friction effect is too simplified. It is, however, only used when checking for governing physical behaviour and it is therefore found to be sufficient.

The result for a downward inclined pipe is given in figure 3.1. The indicator bar to the right represents the colour display for the volume fraction, where 0 (blue) refers to pure liquid and 1 (red) refers to pure gas.

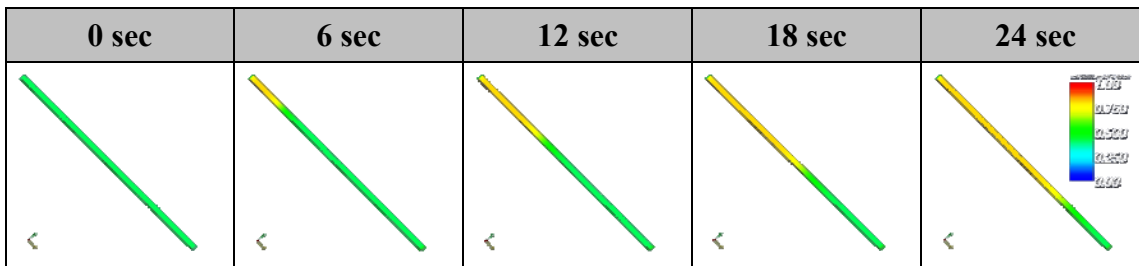


**Figure 3.1. Distribution of volume fraction in a downward inclined pipe.**

It is seen from figure 3.1 that gas is concentrated at the top and liquid in the lower part of the pipe. The high gas fraction at the top is not because the gas drifts upwards but because it flows at a relatively low velocity and thereby it occupies a larger volume than the liquid. The liquid will, due to gravity, be accelerated to a higher velocity and thereby occupy a smaller volume. The gas flows upwards in the lower part of the pipe, due to buoyancy effect.

An additional test with corresponding boundary conditions has been performed for an upward inclined pipe. The result is presented in figure 3.2.

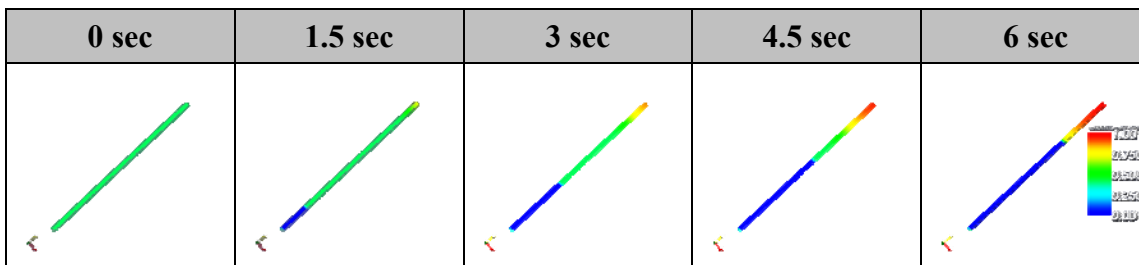


**Figure 3.2. Distribution of volume fraction in an upward inclined pipe.**

It can be seen from figure 3.2 that the liquid accumulates in the bottom part of the pipe and the gas in the upper part of the pipe. The accumulated liquid is partly due to the liquid

feed from the inlet and partly due to the liquid flowing backwards in the upper part of the pipe.

Based on the results discussed above it can be concluded that the model are capable of capturing the buoyancy effect due to density differences.

### 3.6.2 Static pressure

The static pressure is examined by two methods. One is to investigate the pressure profile through the pipe with variations in the pipe inclination. Another is to vary the volume fraction and thereby mixture density to and check for static pressure variations.

The pressure distribution should vary with the pipe inclination due to the change in liquid height. The tests are performed using same conditions as given in table 3.1. The pipe length is 50 meters.

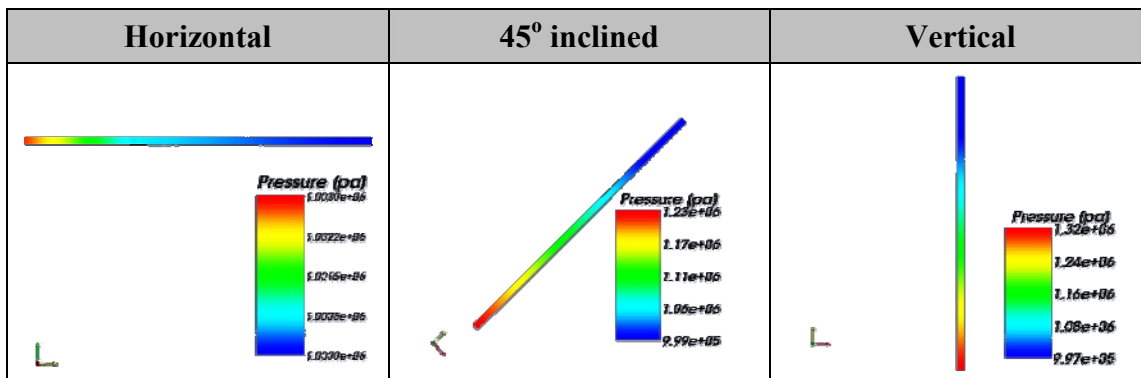


Figure 3.3. Pressure profiles for three pipe inclinations.

It can be seen from figure 3.3 that the pressure profile varies significantly with the change in static head. For the horizontal case a pressure difference of approximately 30,000 Pascal which can be explained with pressure drop strictly due to friction. For the inclined case and the vertical case the pressure differences are 240,000 and 350,000 Pascal, respectively. This implies that an additional pressure drop to friction loss occurs. This is assumed to be the static pressure.

By varying the alpha volume fraction the mixture density should vary and thereby the static head. The results for three different gas volume fractions are presented in figure 3.4.

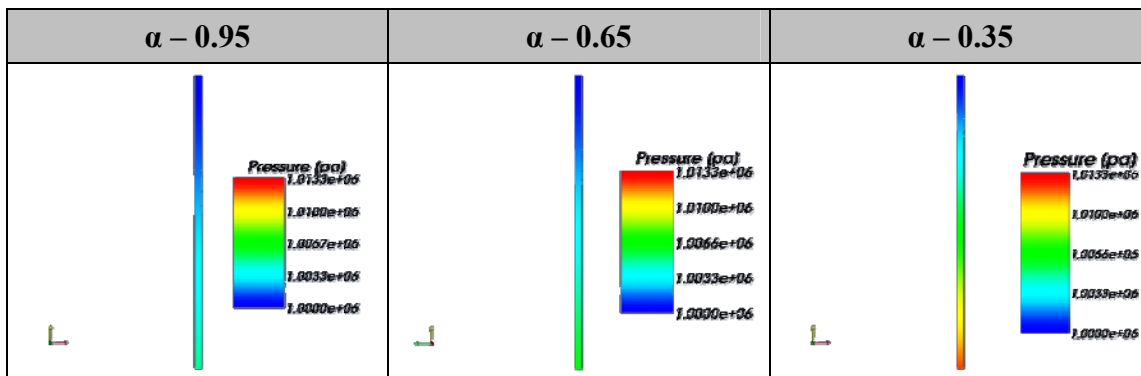


Figure 3.4. Pressure profiles for three gas volume fractions.

It can be seen from figure 3.4 that the pressure is significantly higher for the case with a lower void fraction. For the case with 0.95 gas volume fraction the pressure difference are 3,300 Pascal, while for the case with 0.35 gas volume fraction it is 13,300 Pascal.

It can be concluded, based on above discussed results, that the model is capable of implement static pressure. It is shown that the static pressure varies with liquid height and void fraction.

### 3.6.3 Friction Impact

The impact of the friction is examined by running cases with different factors representing the friction factor. This is done to make sure that there exist a relation between this factor and the friction influence on the model. It is examined by letting the two fluids flow through a pipe at different velocities and with different friction factors.

By varying the friction factor constant, e.g. corresponding to different pipe types the pressure profile should vary. A larger friction factor constant should result in increasing momentum transfer to the wall and thereby an increased pressure drop. The results for three different friction factor constants are given in figure 3.5.

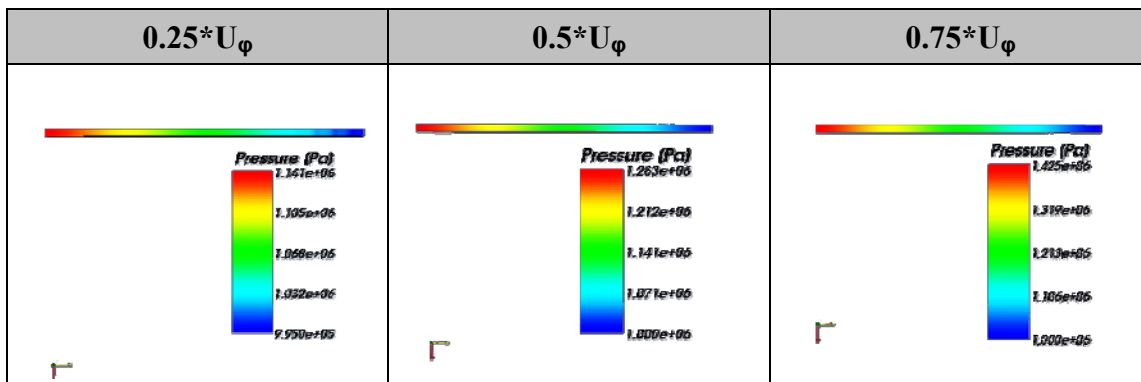


Figure 3.5. Pressure profiles for three different friction constants.

It can be seen from the pressure profiles in figure 3.5 that an increase in friction factor results in increased pressure drop. The pressure drops for friction constant 0.25, 0.5 and 0.75 are approximately 141,000 Pascal, 283,000 Pascal and 425,000 Pascal respectively. It is noted that the pressure drop holds a proportional relationship to the friction factor.

Increasing the velocity results in increased momentum transfer between the fluids and the wall and thereby an increased pressure drop. The pressure profiles for three different velocities are given in figure 3.6.

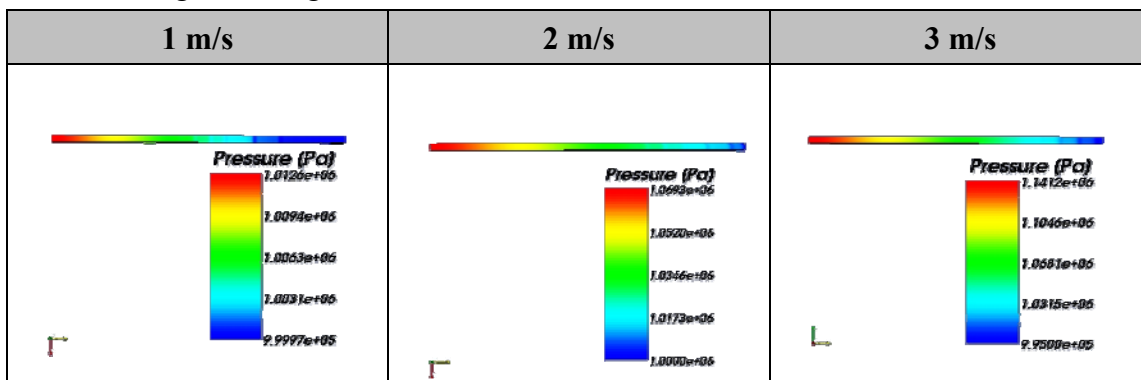


Figure 3.6. Pressure profiles for three different velocities.

It can be seen from the results in figure 3.6 that increased velocities clearly results in increased pressure drop. The pressure drops for 1, 2, and 3 m/s are 12,000 Pascal, 49,300 Pascal and 141,200 Pascal, respectively. It is noted that the pressure drop hold a non-linear

relationship to the velocity. This is in agreement with the fact that the friction loss is a parabolically function of velocity.

Based on the discussed results above for the influence of friction on the pressure distribution through the pipe, it is concluded that the model are capable of capturing friction loss.

### **3.6.4 Summary of test**

Based on the testing carried out to secure the capturing of basic physics it is concluded that the model are validated and further implementation for simulating severe slugging can be incorporated.



## 4 Friction model

In this section it is shown how friction can be implemented into model. As previously stated the one-dimensional model is based on semi-empirical modelling regarding momentum transfer. This is because the friction is not modelled as actual wall functions and interface function. It is modelled by implementing it as a source term based on approximate friction factors.

Three different momentum transfers has to be modelled; momentum transfer between the gas and pipe wall, momentum transfer between liquid and pipe wall, and momentum transfer between the phases.

As described in appendix A – Flow Patterns; two-phase flow can occur in different flow regimes. Different flow regimes will result in different momentum transfer rates. The flow regime must therefore initially be determined. This can be an exhaustive and complicated task. As severe slugging occurs at low flow rates it can be justified that stratified flow is assumed for the feed pipe. The friction factor determined for the feed pipe will also be utilized for the riser section. One may argue that this is incorrect, but it is considered relatively simple to implement a more correct friction model for the riser section and therefore attention are given to more complex issues. The model for momentum transfer in the riser system, however, can be implemented in same manner as for the feed pipe.

### 4.1 Momentum transfer between gas and pipe

The momentum transfer between the gas and the pipe wall can be expressed by considering the shear forces. The shear force is given by equation 4.1.

$$\tau = \frac{f \rho u_r^2}{2} \quad (4.1)$$

The challenging task is to determine a proper friction factor. Taitel and dukler<sup>12</sup> suggested that the gas was evaluated as for a closed-duct flow. From this the friction factor can be evaluated as

$$f_{GW} = C_G \left( \frac{D_G u_G}{\nu_G} \right)^{-m} \quad (4.2)$$

Where  $C_G$ : Coefficient    laminar – 16    turbulent – 0.046

$m$ : Coefficient    laminar – 1.0    turbulent – 0.2

$\nu_G$ : Kinematic viscosity

$D_G$ : Hydraulic diameter

The hydraulic diameter for a closed-duct flow is given as;

$$D_G = \frac{4A_G}{S_G + S_i} \quad (4.3)$$

The variables in equation 4.3 can best be evaluated by considering the cross-sectional geometry for stratified flow depicted in figure 4.1.

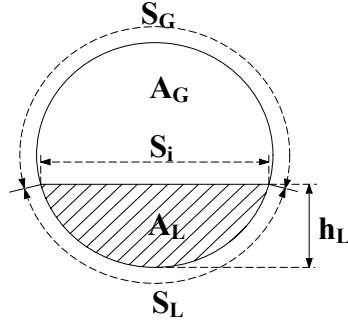


**Figure 4.1. The geometry for the stratified flow.**

The cross section area occupied by the gas phase can be calculated as;

$$A_G = \alpha \cdot A_{Pipe} \quad (4.4)$$

The gas-wall interface and gas-liquid interface is expressed by the liquid height, depicted as  $h_L$  in figure 4.1. The gas-wall interface is expressed in equation 4.5.

$$S_G = D \cdot \cos^{-1} \left( 2 \cdot \left( \frac{h_L}{D} \right) - 1 \right) \quad (4.5)$$

The gas-liquid interface is expressed in equation 4.6.

$$S_i = D \cdot \sqrt{1 - \left( 2 \cdot \frac{h_L}{D} - 1 \right)^2} \quad (4.6)$$

Since only the gas volume fraction and pipe area is available, it is necessary to express the liquid height as a function of this. The relationship between these is given in equation 4.7.

$$\alpha \cdot A = A_L = D^2 \cdot 0.25 \left[ \cos^{-1} \left( 2 \cdot \frac{h_L}{D} - 1 \right) \right] - 0.25 \left[ \left( 2 \cdot \frac{h_L}{D} - 1 \right) \cdot \sqrt{1 - \left( 2 \cdot \frac{h_L}{D} - 1 \right)^2} \right] \quad (4.7)$$

It can be seen from equation 4.7 that an expression for the liquid height based on the gas cross-sectional area fraction will become an implicit function. The solution to this implicit function has to be found using a numerical method which will significantly increase the calculation time as this calculation is carried out numerous times. For this reason it is chosen to express the liquid height based on an explicit function. This is done by using a third degree polynomial function to describe it. The relationship between the dimensionless liquid fraction  $A_L/D^2$  and dimensionless liquid height  $h_L/D$  is illustrated in figure 4.2.

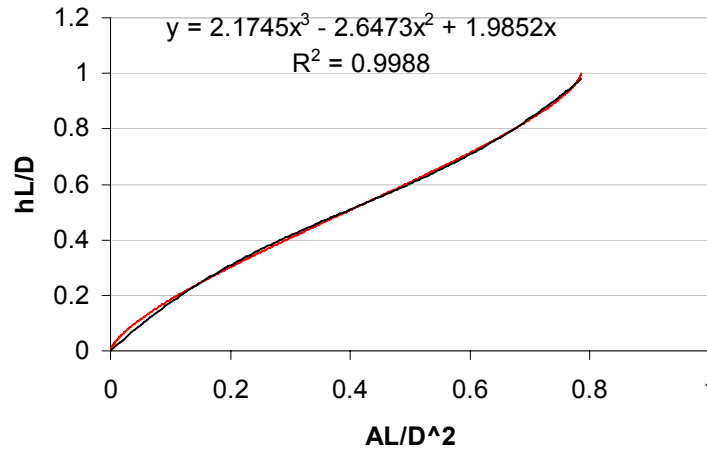


**Figure 4.2. The relationship between dimensionless liquid height and dimensionless liquid area.**

By fitting a polynomial function an explicit expression is obtained. The liquid height can therefore be calculated by equation 4.8.

$$h_L = D \cdot (2.1745 \cdot A_{Ldim}^3 - 2.6473 \cdot A_{Ldim}^2 + 1.9852 \cdot A_{Ldim}) \quad (4.8)$$

Where  $A_{LDim}$  is the dimensionless diameter of the liquid area. Hence, can the friction factor be determined.

The area on which the friction acts is given by the product of the length  $S_G$  and the mesh length. This is given by equation 4.9.

$$\tau_{GW} \cdot A_{Gas-Wall} = \tau_{GW} \cdot S_G \cdot L_{Mesh} = F_{Gas-Wall} \quad (4.9)$$

From the r.h.s of equation 3.30

$$\dots + \frac{F_{fric-a}}{\alpha_a \cdot \rho_a} + \frac{M_a}{\alpha_a \rho_a} = \dots + \frac{F_{Gas-Wall}}{\alpha_a \cdot \rho_a} + \frac{F_{Gas-Liquid}}{\alpha_a \cdot \rho_a} \quad (4.10)$$

It is obvious that the impact from the friction is dependent on the volume on which it acts. An equal friction force will have a larger influence on the momentum for a small volume than for a larger. For this reason the friction term is divided by the relevant volume.

$$\dots + \frac{F_{fric-a}}{\alpha_a \cdot \rho_a} + \frac{M_a}{\alpha_a \rho_a} = \dots + \frac{\tau_{GW} \cdot S_G \cdot L_{Mesh}}{\alpha_a \cdot \rho_a \cdot A \cdot L_{Mesh}} + \frac{F_{Gas-Liquid}}{\alpha_a \cdot \rho_a} \quad (4.11)$$

Equation 4.11 can be simplified to equation 4.12.

$$\dots + \frac{F_{fric-a}}{\alpha_a \cdot \rho_a} + \frac{M_a}{\alpha_a \rho_a} = \dots + \frac{\tau_{GW} \cdot S_G}{\alpha_a \cdot \rho_a \cdot A} + \frac{F_{Gas-Liquid}}{\alpha_a \cdot \rho_a} \quad (4.12)$$

## 4.2 Momentum transfer between gas and liquid

The interface between the two fluids is assumed to be stratified smooth. If the gas flows at higher velocity than the liquid, momentum will be transferred from the gas to the liquid. If the liquid flows with the highest velocity momentum will be transferred from the liquid to the gas. The shear force is evaluated as in the previous, as;

$$\tau_{GL} = \frac{f \rho |u_r| u_r}{2} \quad (4.13)$$

Where  $u_r$ : relative velocity.  $u_r = u_a - u_b$

One  $u_r$  is evaluated as an absolute value, while the other is with sign. This ensures that the momentum gets a sign equal to that of  $u_r$ .

It is common practice to assume that the friction factor for the gas-wall interface and gas-liquid interface is equal for low flow rates. By using the same method as for the derivation of the gas-wall interface the r.h.s. of the momentum equation becomes;

$$\dots + \frac{F_{fric-a}}{\alpha_a \cdot \rho_a} + \frac{M_a}{\alpha_a \rho_a} = \dots + \frac{\tau_{GW} \cdot S_G}{\alpha_a \cdot \rho_a \cdot A} + \frac{\tau_{GL} \cdot S_i}{\alpha_a \cdot \rho_a \cdot A} \quad (4.14)$$

## 4.3 Momentum transfer between liquid and pipe

The momentum transfer rate between the liquid and pipe is based on the same method as described above. The r.h.s of the momentum equation is presented in equation 4.15.

$$\dots + \frac{F_{fric-b}}{\alpha_b \cdot \rho_b} - \frac{M_a}{\alpha_b \rho_b} = \dots + \frac{\tau_{LW} \cdot S_L}{\alpha_b \cdot \rho_b \cdot A} + \frac{\tau_{GL} \cdot S_i}{\alpha_b \cdot \rho_b \cdot A} \quad (4.15)$$

## 5 Pipe Inclination

In this section it will be described how to implement the pipe inclination into the model. As it is chosen to model in one dimension it is a challenging task to vary the pipe inclination. Utilizing traditional methods where the geometry is modelled with respect to a constant gravitational acceleration will introduce difficulties in areas where the pipe inclination changes.

Consider the lower elbow in the pipe-riser system, meshed and modelled for one-dimensionality. This system is depicted in figure 5.1.

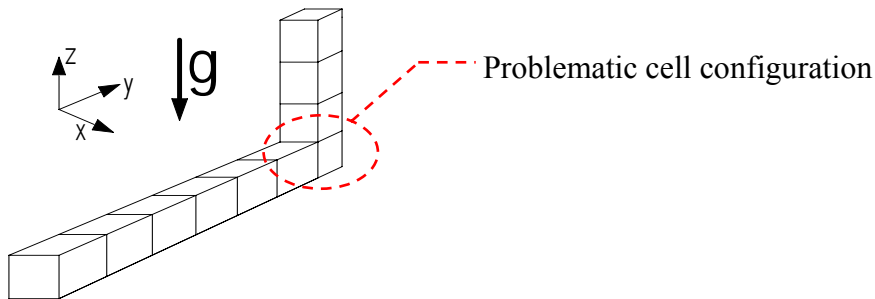


**Figure 5.1. One dimensional case modelled with respect to constant gravity.**

At the horizontal part the flow will have a velocity in the y-direction only. As the flow reaches the elbow a large deceleration will occur in the y-direction. This momentum change has to be transferred to the z-direction which is a problem due to the orthogonal mesh. The problem can possibly be avoided by introducing a non-orthogonal mesh in the area around the lower elbow and setting up a function for the wall. This will, however, probably introduce the need for extra iterations to account for non-orthogonality. Furthermore it is assumed that this method can introduce errors into the model due to the one-dimensionality. This is because a sudden change in the direction of the velocity vector can cause instabilities.

Another option is to model the geometry with respect to a varying gravitational acceleration. This method can be illustrated by figure 5.2.

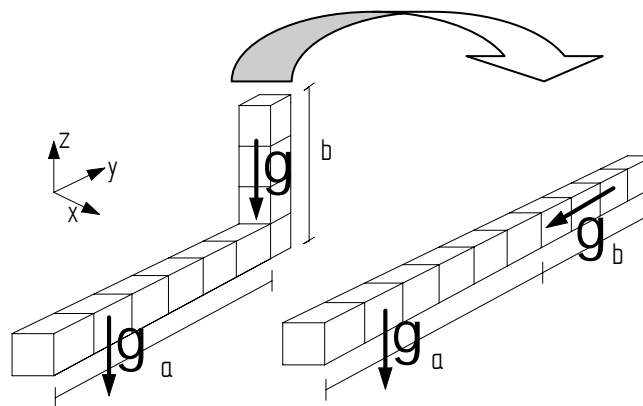


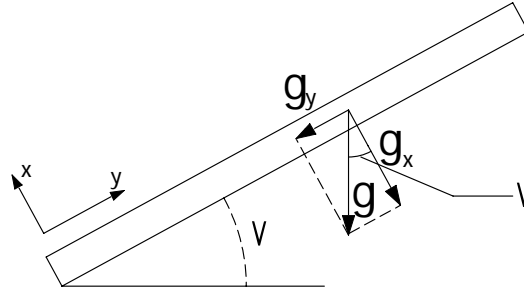
**Figure 5.2. One dimensional case with varying direction of gravity.**

The main idea is to construct the pipe system as one long continuous horizontal system. Any deviation of the pipe geometry from horizontal is then expressed as a variation in the direction of the gravity.

The gravitational acceleration vector is traditionally implemented in OpenFoam as a constant, e.g. a dimension which does not vary with location. This can be written as;

$$g(x, y, z) = g \quad (5.1)$$

Where  $g$ ; Constant vector of magnitude  $9.82 \text{ m/s}^2$  facing downwards



Assuming one-dimensionality, placing coordinate axes relative to pipe inclination, and by decomposing the gravitational vector into an x-component and a y-component, equation 5.1 can be written as;

$$g(x, y, z) = g(y) = g \cdot \sin(v) \quad (5.2)$$

## 6 Review of OpenFOAM

The purpose of this section is to give a short perfunctory description of OpenFOAM. It will clarify the basic structure of OpenFOAM. A more meticulous description of OpenFOAM and its utilities can be found in the guides published by OpenCFD Limited<sup>1011</sup>. OpenFOAM is a C++ library containing predefined operations for pre-processing, solving, and post-processing. OpenFOAM is based on a three dimensional platform and utilises tensor of different ranks to describe the physical entities. The basic approach is to set up a given case and solve this by applying a solver to the case. OpenFOAM is not compatible with windows and therefore it is necessary to apply it to a Linux-based operating system. This can be done by use of an emulator program such as VMware® Workstation if using windows.

### Pre-processing

Pre-processing refers to the operations carried out prior to the calculations. This covers mainly setting up the boundary conditions, initial conditions, mesh, and variables for the calculations. A case directory will as minimum contain three directories 0, constant, and system. The 0 directory contains the initial values of the field variables. The constant directory contains information regarding properties such as gravity and fluid properties. It also contains an additional directory denoted `polyMesh` containing information about the geometry, mesh, and boundary conditions. The system directory contains information required by the solver, e.g. timestep, end time, tolerances, number of correction loops, and selected schemes.

### Solving

Solving refers to the application where iterative calculations are carried out for the field at different time steps. Different standard solvers can be utilized for this operation as well as modified solvers.

### Post-processing

Post-processing refers to application used subsequent to the solving sequence. This involves data processing using reader modules, e.g. `paraView`. Another option is to generate log files.

---

<sup>10</sup> “OpenFOAM – User Guide”

<sup>11</sup> “OpenFOAM – Programmers Guide”

## 7 OpenFoam Solver

In this section it will be described how the new solver is implemented in OpenFOAM. The solver is based on the theory previously described. It is chosen to name the new solver 1DslugFoam, which is in accordance with the existing solver names. The program code will be presented and the link between the code and theory will be established. The clarification of the programming structure is important due to the future work of introducing additional conditions to the programme, e.g. compressibility, modified friction models, and consequences from slug preventing process equipment.

The basic structure of the solver is found in the solver directory denoted 1DslugFoam. The directory can be found on the associated CD. The directory consists of 1 main source file and 9 header files. In addition a directory used for the compilation of the solver and linking the solver to libraries is found in the solver directory. The solver directory structure is depicted in figure 7.1.

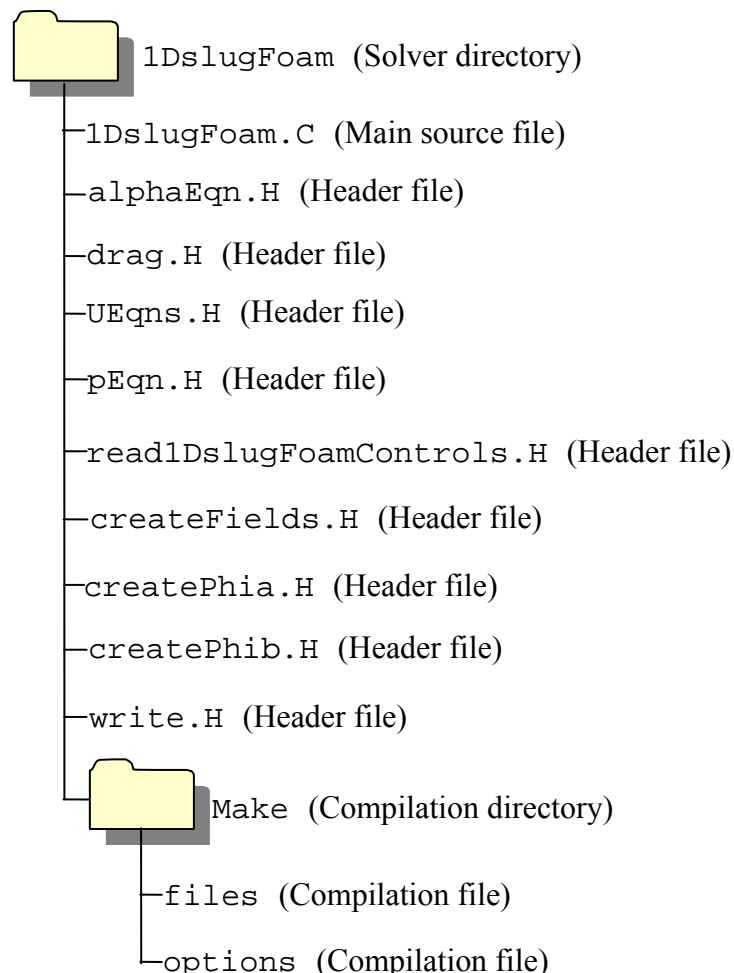


**Figure 7.1. The solver directory structure.**

In addition to the files presented above, a dependency file is created when compiling the solver. This dependency file lists the references between the solver and header/source files.



The function of the file and programming code will be explained in the following. References will be made to the previously described theory on which the solver is based on.

The structure of the following sections is an introductory explanation before presenting the actual code. All OpenFoam code will be presented in a frame, and the code is presented using Courier New as character. An example is given below.

`OpenFoam code`

The following sections will go through the main files which constitutes the solver.

## 7.1 1DslugFoam

1DslugFoam.C is the main source file of the solver. It contains the main structure for the basic algorithm presented in section 3.5 Solution algorithm. First step in the source file is a reference to fvCFD.H. This is a header file that makes references to basic functions, such as tensor descriptions, time functions and discretisation. A reference to the Switch.H file is also made. This activates the yes/no and true/false functions.

```
#    include "fvCFD.H"
#    include "Switch.H"
```

Next is references made to files which aborts if arguments are not fulfilled. Furthermore is a reference to the element division and time steps made.

```
#    include "setRootCase.H"
#    include "createTime.H"
#    include "createMesh.H"
```

Subsequently, the fields are created. A field is a tensor of any rank that must be calculated for each cell, either at the surface or at the node point. There will be accounted for this in the following.

```
#    include "createFields.H"
```

Next a reference is made for calculating the accumulated continuity error. This error can be linked to the pressure solver tolerance. It is important that the errors are kept at an acceptable low level.

```
#    include "initContinuityErrs.H"
```

All references above are static and are not depending on the timestep. Next stage is to include the time step.

```
for (runTime++; !runTime.end(); runTime++)
{
    #       include "readlDslugFoamControls.H"
    #       include "CourantNo.H"
    #       include "alphaEqn.H"
    #       include "drag.H"
    #       include "UEqns.H"
```

Where `readlDslugFoamControls.H` are a function that looks up the number of correction loops for alpha and if alpha should be corrected by recalculating `alphaEqn.H` after the pressure equation. `CourantNo.H` calculates the courant number. The courant number is the ratio between the timestep and mesh size multiplied with the phase velocity. The `alphaEqn.H`, `drag.H`, and `UEqns.H` will be accounted for in the following sections.

The next step in the main source file is the initiation of the PISO loop.

```
    for (int corr=0; corr<nCorr; corr++){
#       include "pEqn.H"
        if (correctAlpha) {
#       include "alphaEqn.H"    }}
```

The numbers of loops carried out in the PISO loop is determined by `nCorr` which is set up in the case directory. The last reference made in the main source file is to `write.H` which writes the relative velocity to the case directory.

```
#       include "write.H"
Info<<"ExecutionTime = " << runTime.elapsedCpuTime()<<"s"
    <<"ClockTime = " << runTime.elapsedClockTime()<<"s"
<< nl << endl; }
Info<< "End\n" << endl; return(0); }
```

The main source file presents the clocktime and execution time. The ratio between these times indicates the processor utilisation.

## 7.2 createFields.H

The first reference to a solver-dependent file is made to `createFields.H`. This file creates geometric fields of the scalar-type or vector type. Fields for the gravity term, gas fraction (alpha), and liquid fraction (beta) are created and the code is presented in the following.

The expression `runTime.timeName()` and mesh controls that the field are time and location dependent. `MUST_READ` ensures that the initial value of alpha and g are taken from the 0-directory in the case. `NO_WRITE` and `AUTO_WRITE` controls if the calculated or constant values are written to the case directory for each written timestep.

```

Info << "\nReading g" << endl;
volVectorField g
(
    IOobject (
        "g",
        runTime.timeName(),
        mesh,
        IOobject::MUST_READ,
        IOobject::NO_WRITE ), mesh    );

Info<< "Reading field alpha\n" << endl;
volScalarField alpha
( IOobject (
    "alpha",
    runTime.timeName(),
    mesh,
    IOobject::MUST_READ,
    IOobject::AUTO_WRITE), mesh    );

volScalarField beta
( IOobject (
    "beta",
    runTime.timeName(),
    mesh,
    IOobject::NO_READ,
    IOobject::NO_WRITE ), scalar(1) - alpha );

```

Fields are also created for the pressure, phase velocities and fluxes. The createFields.H file also includes references to the transport properties directory situated in the case directory. An example for this is as follows.

```

dimensionedScalar rhoa
( transportProperties.lookup("rhoa") );

dimensionedScalar rhob
( transportProperties.lookup("rhob") );

```

In addition, values for kinematic viscosity, pipe geometry, and laminar/turbulent factors are also obtained.. The last task carried out in the file is the calculation for the static pressure.

```

Info<< "Calculating field g.h\n" << endl;
volScalarField gh("gh", g & mesh.C());
label pRefCell = 0;
scalar pRefValue = 0.0;
setRefCell(p, mesh.solutionDict().subDict("PISO"), pRefCell,
pRefValue);

```

## 7.3 alphaEqn.H

The continuity equation is solved in alphaEqn.H. The courant number is also calculated for the relative phase flux. This courant number shows if the relative velocity between the phases is too high compared to the ratio between the time steps and mesh size.

```

surfaceScalarField phir = phia - phib;
Info<< "Max Ur Courant Number = " << ( max (
mesh.surfaceInterpolation::deltaCoeffs()*mag(phir)
    /mesh.magSf()
    )*runTime.deltaT()
    ).value()
<< endl;

```

Where the term `mesh.surfaceInterpolation::deltaCoeffs()` refers to the reciprocal value of the distance between the cell centres.

The gas volume fraction is based on the discretised continuity equation.

$$\left\| \frac{\partial [\alpha_a]}{\partial t} \right\| + \left\| \nabla \cdot \left( \phi [\alpha_a]_{f(\phi, scheme)} \right) \right\| + \left\| \nabla \cdot \left( \phi_{ra} [\alpha_a]_{f(\phi_{ra}, scheme)} \right) \right\| = 0 \quad (7.1)$$

The liquid fraction is afterwards calculated based on alpha.

```

Word scheme ("div(phi,alpha)");
for (int acorr=0; acorr<nAlphaCorr; acorr++) {
fvScalarMatrix alphaEqn
    ( fvm::ddt(alpha)
    + fvm::div(phi, alpha, scheme)
    + fvm::div(-fvc::flux(-phir, beta, scheme), alpha, scheme );
    alphaEqn.solve();

beta = scalar(1)-alpha
alpha = 0.5*(scalar(1) + pow((scalar(1) - beta),2) - pow((scalar(1) -
alpha),2)); }

```

The last term in the alpha equation is implemented for iterative purpose. The term  $\left\| \nabla \cdot \left( \phi_{ra} [\alpha_a]_{f(\phi_{ra}, scheme)} \right) \right\|$  is non-linear and therefore is an iterative process required. This does not guarantee boundedness. The last term in the code is therefore introduced to ensure boundedness. The word `scheme` refers to a scheme defined in the case file `fvschemes` later described. `Fvm` refers to a list of static functions used for the differential operator. It calculates implicit derivatives and creates a matrix.

## 7.4 Drag.H

All terms used for the friction model is calculated in the file `drag.H`. Here is both friction factors and flow geometry based on liquid height calculated. The liquid height is based on a dimensionless expression for the cross-sectional liquid area and calculated by an approximative polynomial, as described in section 4 Friction model.

```
volScalarField Ab = beta*A;
volScalarField Abdim = Ab/(D*D);
volScalarField hldim = 2.1758*pow(Abdim,3) - 2.6485*pow(Abdim,2)
+ 1.9854*Abdim;
```

Subsequently is the remaining flow geometric conditions calculated. Da and Db are the hydraulic diameter for the gas and liquid, respectively. Sa, Sb, Si are the interface between gas-pipe, liquid-pipe and gas-liquid, respectively.

```
volScalarField Si ("Si", sqrt(1-pow(2*hldim-1,2))*D);
volScalarField Sa ("Sa", acos(2*hldim-1)*D);
volScalarField Sb ("Sb", (mathematicalConstant::pi -
(Sa/D))*D);
volScalarField Da ("Da", 4*Aa/(Sa + Si));
volScalarField Db ("Db", 4*Ab/Sb);
```

The friction factors are multiplied with the magnitude of the velocity vector (tensor of rank 1). This is done because the inner product of the vectors would produce a scalar (tensor of rank 0) and the outer product would produce a matrix (tensor of rank 2). It is important to maintain the orientation of the velocity vector in order to determine the direction of the acceleration term due to friction. For this reason the friction factors are multiplied with the velocity magnitude and afterwards, when utilized in the momentum equation, the remaining velocity vector is scaled by this resulting factor.

```
volScalarField fa_magUa ("fa_magUa", C*pow(Da*magUa/nua,-
n)*magUa);
volScalarField fb_magUb ("fb_magUb", C*pow(Db*magUb/nub,-
n)*magUb);
volScalarField fi_magUr ("fi_magUr", C*pow(Da*magUa/nua,-
n)*magUr);
```

This method will introduce a small error since the velocity magnitude used is an old value. This error is, however, assumed to be of acceptable magnitude since no rapid velocity changes are expected.

## 7.5 UEqns.H

The momentum equation without the pressure term is solved in UEqns.H. It is done by initially defining the two velocity matrixes.

```
fvVectorMatrix UaEqn(Ua, Ua.dimensions()*dimVol/dimTime);
fvVectorMatrix UbEqn(Ub, Ub.dimensions()*dimVol/dimTime);
```

Next, the two momentum equations are treated. The interface momentum transfer rate are decomposed into an expression for each phase velocity.

```

UaEqn = ((
    fvm::ddt(Ua)
    + fvm::div(phia,Ua) )
    ==
    - fvm::Sp(fa_magUa/2*Sa/(alpha*D*D/4*mathematicalConstant::pi), Ua)
    - fvm::Sp(fi_magUr/2*Si/(alpha*D*D/4*mathematicalConstant::pi), Ua)
    + fi_magUr/2*Si/(alpha*D*D/4*mathematicalConstant::pi)*Ub ));
UaEqn.relax();

UbEqn = ((
    fvm::ddt(Ub)
    + fvm::div(phib,Ub) )
    ==
    - fvm::Sp(fi_magUr/2*Si/(alpha*D*D/4*mathematicalConstant::pi), Ub)
    - fvm::Sp(fb_magUb/2*Sb/(beta*D*D/4*mathematicalConstant::pi), Ub)
    + fi_magUr/2*Si/(alpha*D*D/4*mathematicalConstant::pi)*Ua );
UbEqn.relax(); }

```

## 7.6 pEqn.H

The pressure term which is left out from the momentum equation is solved in the pEqn.H file. Initially is the phase velocities calculated as  $\overline{U}_\varphi = (M_\varphi)_H^{-1} (M_\varphi)_D$  as stated in section 3.4.3 Momentum corrector equation.

```

volScalarField rUaA = 1.0/UaEqn.A();
volScalarField rUbA = 1.0/UbEqn.A();
Ua = rUaA*UaEqn.H();
Ub = rUbA*UbEqn.H();

```

rUaA is the reciprocal expression for the diagonal matrix. UaEqn.H( ) is the H operator. Subsequently is the fluxes predicted by  $\varphi_\varphi^* = \left( (M_\varphi)_D^{-1} (M_\varphi)_H \right)_f \cdot S_f$ .

```

surfaceScalarField alphaf = fvc::interpolate(alpha);
surfaceScalarField betaf = scalar(1) - alphaf;
phia =
(fvc::interpolate(Ua) & (mesh.Sf()/mesh.magSf()*A)) +
fvc::ddtPhiCorr(rUaA, Ua, phia);
phib =
(fvc::interpolate(Ub) & (mesh.Sf()/mesh.magSf()*A)) +
fvc::ddtPhiCorr(rUbA, Ub, phib);
phi = alphaf*phia + betaf*phib;

```

The term `ddtPhiCorr` removes the divergence of the flux by relating the interpolated velocity to the flux.

The next step taken is the construction of the pressure equation.

$$\left\| \nabla \cdot \left( \alpha_{af} \left( \frac{1}{\rho_a (M_a)_D} \right)_f + \alpha_{bf} \left( \frac{1}{\rho_b (M_b)_D} \right)_f \right) \nabla \bar{p} \right\| = \nabla \cdot (\alpha_{af} \phi_a^* + \alpha_{bf} \phi_b^*) \quad (7.2)$$

The coding initial constructs the surface parentheses before solving the pressure matrix.

```
surfaceScalarField Dp("(rho*(1|A(U)))", alphaf*rUaAf/rhoa +
betaf*rUbAf/rhob);
fvScalarMatrix pEqn (
fvm::laplacian(Dp, p) == fvc::div(phi) );
pEqn.setReference(pRefCell, pRefValue);
pEqn.solve();
```

After solving the pressure equation the fluxes is corrected. `pEqn.flux()` is an expression for the flux. This is divided by the surface parentheses in order to remove the volume fraction.

```
surfaceScalarField SfGradp = pEqn.flux()/mesh.magSf()*A/Dp;
phia -= rUaAf*SfGradp/rhoa;
phib -= rUbAf*SfGradp/rhob;
phi = alphaf*phia + betaf*phib;
```

The last step is to correct the velocities. This is done by a reconstruction procedure where the velocities are obtained from the fluxes.

```
surfaceScalarField phiDraga = rUaAf*(gf & mesh.Sf());
surfaceScalarField phiDragb = rUbAf*(gf & mesh.Sf());
Ua += (fvc::reconstruct(phiDraga - rUaAf*SfGradp/rhoa));
Ub += (fvc::reconstruct(phiDragb - rUbAf*SfGradp/rhob));
U = alpha*Ua + beta*Ub;
```

If the correction of alpha is switched on the alpha equation will hereafter be recalculated with the new velocities and fluxes.

After the construction of the solver it is necessary to compile it using the `wmake` feature. This feature rewrites the solver in a binary language.

## 8 Case structure

This section will go through the case structure where information regarding each specific case is incorporated. Conditions such as fluid property, pipe geometry, time step and mesh size is to be found in the case directory. This means that the most values will vary with each test case. This section will however attempt to deliver a generalised presentation of the case structure. The case structure is illustrated in figure 8.1.

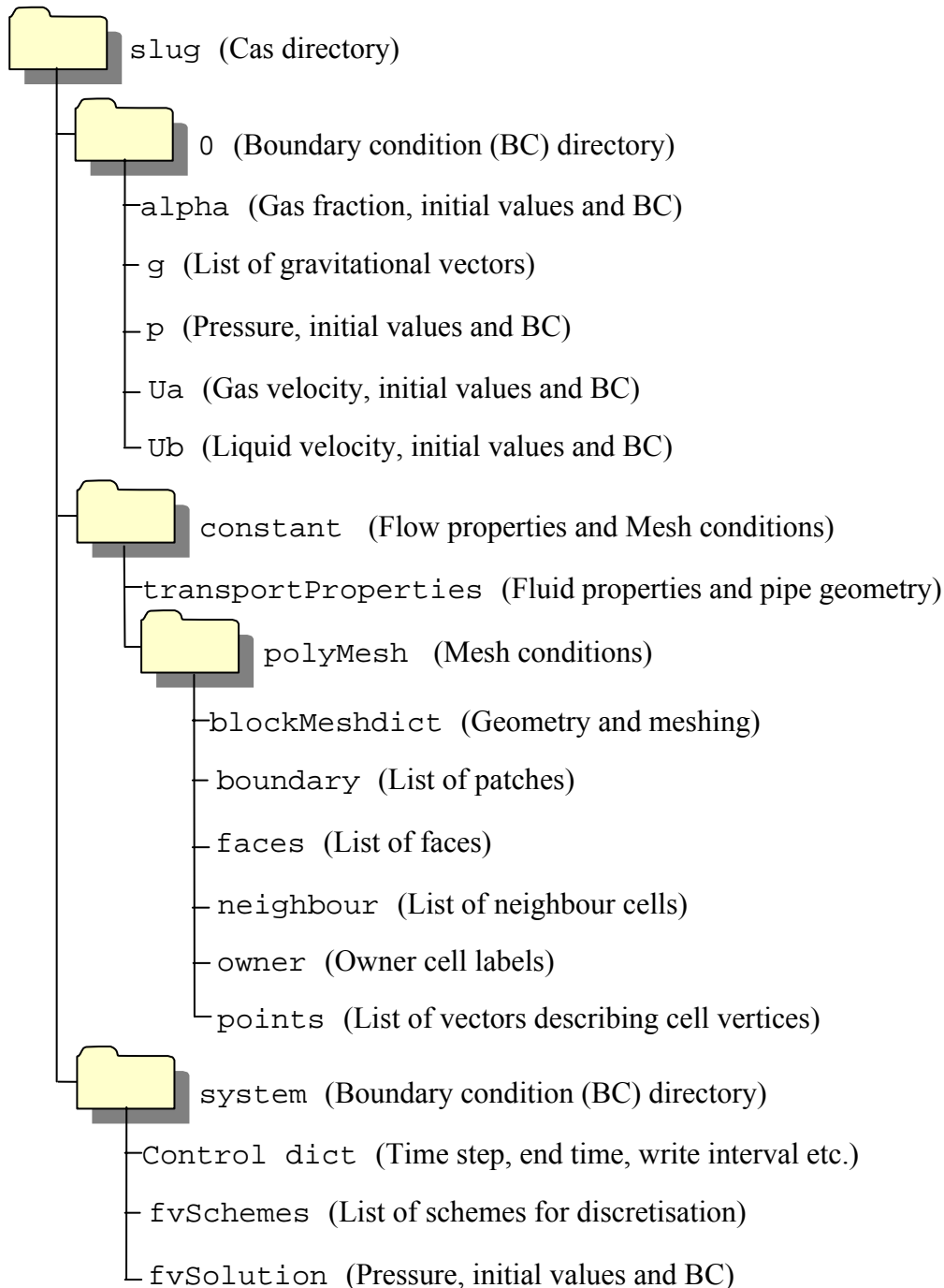


**Figure 8.1. The case directory structure.**



The case directory is as minimum comprised of three main directories: 0, constant, and system. In addition will the solver store all written time steps in the directory. The purpose and examples for the script of each directory will be presented in the following.

## 8.1 0 – directory

The 0 directory contains 5 files, each containing initial values and boundary conditions for patches. The files refer to the gas volume fraction scalars  $\alpha$ , the gravitational acceleration vectors  $\mathbf{g}$ , the pressure scalars  $p$ , the gas phase velocity vectors  $\mathbf{U}_a$ , and the liquid phase velocity vectors  $\mathbf{U}_b$ .

### 8.1.1 $\alpha$

An example of the file containing the dimensioned scalar field  $\alpha$  at cell-node is presented below.

```
dimensions      [0 0 0 0 0 0 0];

internalField    uniform 0.4;

boundaryField {
    inlet{
        type      fixedValue;
        value      uniform 0.4;    }
    outlet{
        type      zeroGradient;    }
    frontAndBack{
        type      empty;           } }
```

The inlet value of the gas fraction is set to 0.4. This value, along with the phase velocity, controls the inlet fraction of the gas into the system. `frontAndBack` is used for the outside patches surrounding the cells. This feature is normally used when treating two-dimensional cases. The outlet type `zeroGradient` refers to a boundary condition where the normal gradient is zero and thereby ignoring the effect of an outlet.

### 8.1.2 $\mathbf{g}$

An example of the file containing the dimensioned vector field  $\mathbf{g}$  at cell-node is presented below.

```

dimensions      [0 1 -2 0 0 0 0];
internalField    nonuniform List<vector>
7 (
(-6.94 6.94 0)
(-6.94 6.94 0)
(-6.94 6.94 0)
(-6.94 -6.94 0)
(-6.94 -6.94 0)
(-6.94 -6.94 0)
(-6.94 -6.94 0));
boundaryField
{ inlet {
    type          fixedValue;
    value          uniform (-6.94 6.94 0); }
  outlet {
    type          fixedValue;
    value          uniform (-6.94 -6.94 0); }
  defaultFaces    { type      zeroGradient; }
}

```

Due to the fact that the orientation of the gravity vector varies within the internal field it is necessary to present it as a non-uniform list. Here the number 7 following `internalField nonuniform List<vector>` refers to the internal number of nodes. This means that a unique vector is assigned to each node and therefore the following number of vectors should correspond to the number of nodes.

### 8.1.3 p

The file containing initial values and boundary conditions for the pressure is `p`. It is chosen to define the outlet pressure (separator pressure) and set the inlet type to `zeroGradient`.

```

dimensions      [1 -1 -2 0 0 0 0];
internalField    uniform 1000000;
boundaryField
{ inlet {
    type          zeroGradient; }

  outlet {
    type          fixedValue;
    value          uniform 1000000; }

  frontAndBack {
    type          empty; } }

```

The outlet pressure is set to 1000000 Pa or 10 bars.

### 8.1.4 Ua and Ub

The OpenFOAM code for the phase velocities is given below. Only one code is presented, because they are of similar type.

```

dimensions      [0 1 -1 0 0 0 0];
internalField    uniform (0 0.5 0);
boundaryField {
    inlet {
        type          fixedValue;
        value          uniform (0 0.5 0); }
    outlet{
        type          zeroGradient; }
    frontAndBack {
        type          empty;}}

```

The initial value and inlet value are 0.5 m/s.

## 8.2 constant

The constant directory is comprised of the file `transportProperties` and the directory `polyMesh`. The file `transportProperties` contains information for the fluid properties and pipe geometry. The `createFields.H` header file is linked to this file and the `createFields.H` looks up the values presented below.

```

//Fluid properties
rhoa  rhoa [1 -3 0 0 0 0 0] 10;
rhob  rhob [1 -3 0 0 0 0 0] 800;
nua   nua  [0 2 -1 0 0 0 0] 1.6e-05;
nub   nub  [0 2 -1 0 0 0 0] 1e-6;
// Geometry
D      D    [0 1 0 0 0 0 0] 0.3;
A      A    [0 2 0 0 0 0 0] 0.07068375;
// Friction coefficients
n      n    [0 0 0 0 0 0 0] -0.2;
C      C    [0 0 0 0 0 0 0] 0.046;

```

The main file in the directory `polyMesh` is `blockMeshDict`. This file is the master file which dictates the content of the additional files; `boundary`, `faces`, `neighbour`, `owner`, and `points`. The initial coding for `blockMeshDict` is presented below.

```

convertToMeters 1;
Vertices (
    (0 0 0)
    (2 0 0)
    (2 1000 0)
    (0 1000 0)
    (0 0 2)
    (2 0 2)
    (2 1000 2)
    (0 1000 2) );
blocks( hex (0 1 2 3 4 5 6 7) (1 1000 1) simpleGrading (1 1 1) );

```

The computational domain is defined by the 8 vertices, given as coordinates in a Cartesian system. This computation domain is depicted in figure 8.2.

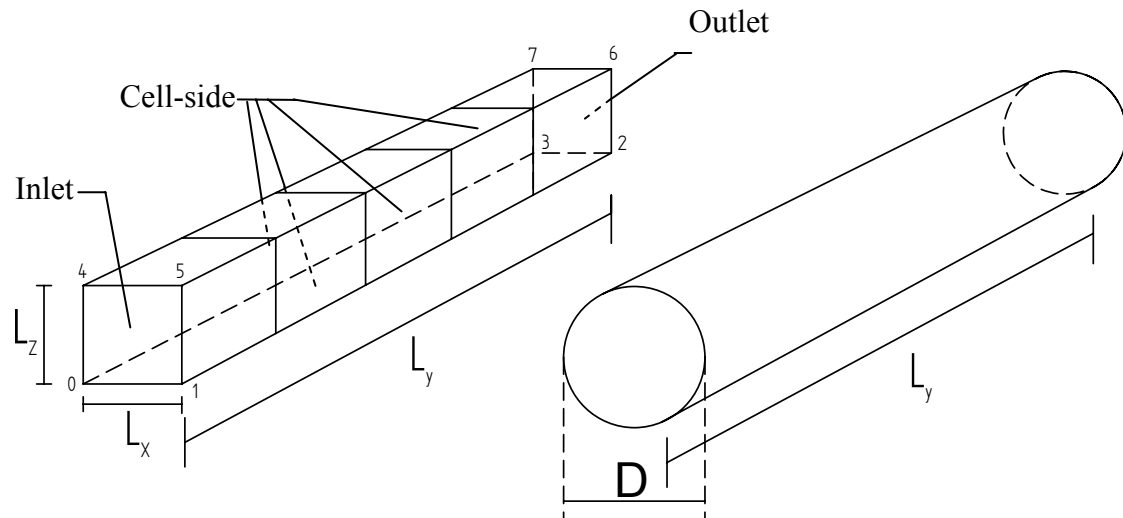


**Figure 8.2. Computational domain and pipe geometry.**

To guarantee a correct transformation between velocity and flux and to ensure correct discretisation it is important to set the value of  $L_z$  and  $L_x$  so that the products equals the cross sectional area of the pipe.  $L_x$  is the first value in the vertices coordinates and  $L_z$  is the second. The third value  $L_y$  must correspond to the total pipe length, this means both feed pipe and riser.

This can be written as;

$$L_y = L_{feed\_pipe} + L_{riser\_pipe}$$

$$L_x \cdot L_z = \frac{\pi}{4} \cdot D^2$$

The `blocks` function divides the domain into hexagonal elements. The subsequent parenthesis defines the volume based on the vertices. The following parenthesis dictates the number of elements the domain is divided into. The last parenthesis `simpleGrading` dictates uniform expansion ratio.

The next piece of code defines the inlet, outlet, and the sides of the cells. The inlet and outlet are defined as patches, while the side of cells are defines as `frontAndBack`.

```
edges( );

patches(
    patch inlet (
        (1 5 4 0))
    patch outlet (
        (3 7 6 2))
    empty frontAndBack (
        (0 4 7 3)
        (2 6 5 1)
        (4 5 6 7)
        (3 2 1 0)));
mergePatchPairs();
```

## 8.3 system

The system directory contains all relevant information that dictates the calculation process. It consists of three files, `controlDict`, `fvSchemes`, and `fvSolution`. `controlDict` dictates time related constants, `fvSchemes` assigns an appropriate discretisation scheme to the finite volume notation, and `fvSolution` specifies tolerances, linear equation solvers and algorithm constants.

### 8.3.1 controlDict

The `controlDict` file controls the timestep, write interval and the time domain for which the calculation is carried out for.

### 8.3.2 fvSchemes

`fvSchemes` assigns an appropriate numerical scheme for the finite volume terms in the solver. The finite volume terms in the `1DslugFoam` solver are, on the whole, the time derivatives, gradients, convection, laplacian, and the interpolation terms. It is possible to assign the schemes as default to a finite volume term group, e.g. time derivatives or to assign a specific discretisation scheme to a particular term.

#### ddtSchemes

`ddtSchemes` assigns a numerical scheme to the first order time derivative. The discretisation schemes for time derivative are based on two governing methods; Euler implicit and backward differencing. Euler implicit is first order accurate because it only uses one old value, while backward differencing is second order accurate because it uses both the old value and the previous before this. Because Backward differencing does requires a larger computational data storage and extra calculation time and because it is assumed that Euler implicit is accurate enough Euler is chosen.

#### gradSchemes

`gradSchemes` assigns a numerical scheme to the gradient term. The discretisation schemes are based on three basic methods; Gauss integration, least squares method and normal surface gradient method. Gauss integration is based on the Gauss theorem which relates the outward flux to the divergence inside the volume. The least squares method extrapolates a value to a neighbour cell using the gradient. It hereafter minimizes the error between the extrapolated value and the value of the neighbour by varying the gradient. The surface normal gradient method determines the gradient value by subtracting the cell value and neighbour value and dividing with the distance.

The latter method is chosen because the one-dimensionality guarantees orthogonally meshes and the solution can there is therefore no need to correct for this. This results in an accurate and simple term.

#### Convection

`divSchemes` assigns a numerical scheme to the convection term. These schemes are of great importance because they take part in the boundedness of the volume fractions. Gauss is the only choice of divergence scheme but a number of the convection-specific interpolation methods can be chosen. These interpolation methods are mainly based on

three major categories; Centered schemes, Upwind convection schemes, and Normalized Variable Diagram (NVD). Centered schemes are based on central differencing where the face value are direct related to node value and neighbour value with respect to the distances. Upwind determines the face value based on the direction of the flow by simply transferring the node value to the cell face. The NVD method normalizes the value so the value of interest at the neighbouring cell becomes 1 for the downstream cell and the upstream value becomes 0. The face value can hereafter be described as a function of the cell of interest.

The boundedness of alpha is conserved by using a limited scheme which treats the convection with respect to alpha which ranges only from 0 to 1. For this reason is `limitedLinear01` scheme chosen for the `div (phi, alpha)` term. This scheme is a subgroup to central differencing. Central differencing is also chosen to the remaining convection terms. The `limitedLinear01` can also be classified as a Total Variation Diminishing (TVD).

### Laplacian

As for convection, Gauss integration is the only scheme which can be used. Central differencing is chosen as interpolation. The scheme can be corrected in order to account for non-orthogonal mech. The one-dimensional mesh does, however, provide possibility to leave the laplacian term in the pressure equation uncorrected.

### Interpolation

It is chosen to set the interpolation for the `fvc::interpolate()` function to linear. Upwind interpolation would result in a very stable calculation, but the flow conditions results in the occurrence of two opposite directed fluxes at neighbouring cells. This will rule out upwind interpolation.

### 8.3.3 fvSolution

Specifications for the linear equation solvers are found in the `fvSolution` file. It dictates the solver which is used for solving the matrixes. There are basically three linear solvers; Preconditioned Conjugate Gradient (PCG), solver using a smoother, and Geometric Algebraic Multi Grid (GAMG).

It is chosen to use the PCG solver for matrixes, except the alpha matrix. This is because the alpha matrix is asymmetric and therefore is a Preconditioned BI-Conjugate Gradient (PBICG) solver utilized. PCG solvers conjugate the values with respect to the matrix and perform iterations. The PBICG solver utilizes non-linear conjugation methods.

When utilizing a PCG or PBICG a preconditioner has to be chosen. A preconditioner is an additional matrix which is multiplied on the original matrix to achieve faster convergence. DIC is applied for the symmetric PCG and DILU for the asymmetric PBICG.

The tolerances are also specified in `fvSolution`. Two tolerances must be defined. The tolerance is based on the residual, e.g. the difference between the l.h.s. and r.h.s. of the matrix. This can be evaluated by both the residual and the relative residual. The relative residual relates the current residual to the initial residual. It is chosen to evaluate the tolerance by the residual.

## 9 Simulation of pipe-riser system

In this section are two simulation of the pipe-riser system presented. The first simulation is performed on a system where the conditions should guarantee a steady state system. The second simulation is performed on a system where the conditions should ensure an unstable system – severe slugging.

### 9.1 Simulating stable system

This section will present a simulation of a stable pipe-riser system is performed. The stability of the system is guaranteed by the equations presented in section 2.4 Stability Criterion. The analysis of the simulation is subdivided into

- Initial conditions
- Processing
- Results

#### 9.1.1 Initial conditions

The pipe-riser system is illustrated in figure 9.1.

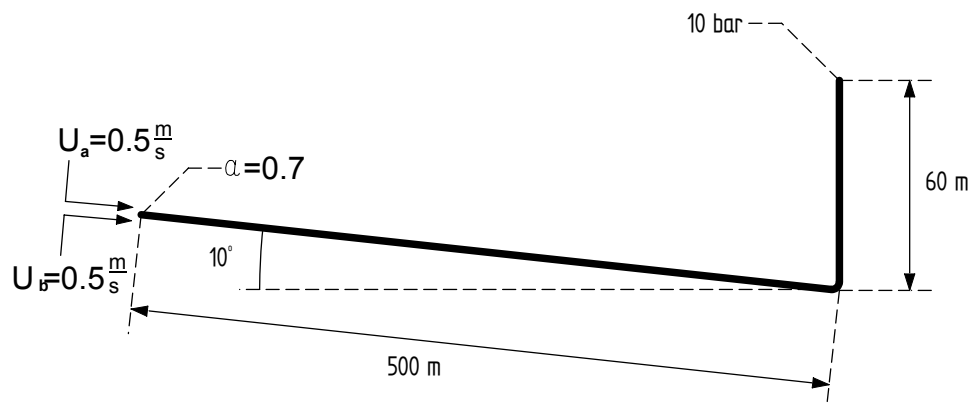


Figure 9.1. Stable pipe-riser system

The initial values and boundary conditions for the test case are presented in table 9.1.

Table 9.1. Initial values and boundary conditions.

	$\alpha$	$U_a$	$U_b$	$p$
<b>Internal value</b>	0.7 [-]	0.5 [m/s]	0.5 [m/s]	10e06 [Pa]
<b>Inlet</b>	0.7 [-]	0.5 [m/s]	0.5 [m/s]	zeroGradient
<b>Outlet</b>	zeroGradient	zeroGradient	zeroGradient	10e06 [Pa]

The properties of the fluid, pipe geometry, time step, and number of cells are presented in table 9.2.

Table 9.2. Pipe diameter, fluid properties and calculation constants

D	$\rho_{\text{Gas}}$	$\rho_{\text{Liquid}}$	$\mu_{\text{Gas}}$	$\mu_{\text{Liquid}}$	$\Delta t$	# of elements
0.3 [m]	10 [kg/m <sup>3</sup> ]	800 [kg/m <sup>3</sup> ]	$1.6 \cdot 10^{-5}$ [m <sup>2</sup> /s]	$1 \cdot 10^{-6}$ [m <sup>2</sup> /s]	0.01 [s]	1120

### 9.1.2 Processing

The solver processed the case for a time domain of 600 seconds with a write interval of 2 seconds. This resulted in a clocktime of 5153 seconds with an execution time of 4933 seconds. The PISO algorithm corrector was set to 2, which is generally assumed to be sufficient. The alpha algorithm corrector was activated and the number of alpha correction loops was set to 2.

The above mentioned calculations conditions resulted in a very low courant number ( $\sim 0.02$ ) for a majority of the calculations. This is necessary due to an extreme gas velocity, which is explained later.

### 9.1.3 Results

The results can be investigated in a number of ways, e.g. raw data log files, paraFoam or third party post-processing tools. It is chosen to examine the results using paraFoam, which is an open source visualization reader module. In addition a sampleDict file is added to the system directory. This file tracks results for specific fields at specified lines, patches or points. The result for the stable pipe-riser system is presented by four

- Volume fraction
- Velocity distribution
- Pressure distribution

#### Volume fraction

The gas volume fraction, alpha, is presented by the visualization tool paraFoam in figure 9.2. It is chosen to represent the analysis by 8 timesteps ranging from 0 to 400 seconds. After approximately 400 seconds the systems becomes stable.

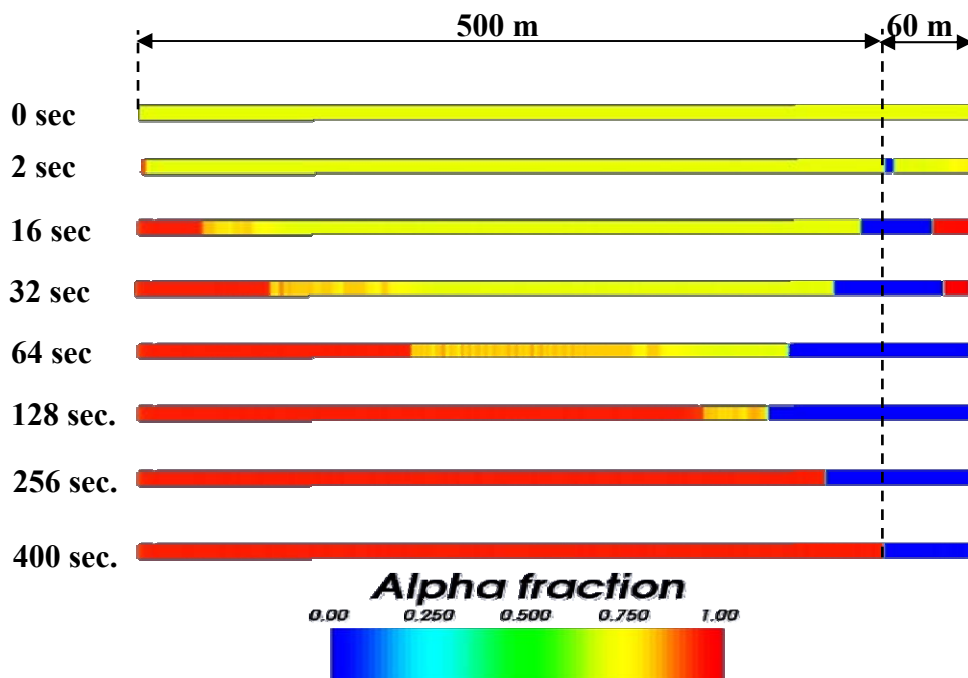


Figure 9.2. Volumetric fraction of gas. The 500 m represents the  $10^\circ$  downward inclined feed pipe. The 60 m represents the vertical riser pipe. 0 refers to pure liquid and 1 refers to pure gas.



## Simulation of pipe-riser system

It can be seen from figure 9.2 that the liquid is accumulated at the lower elbow. The liquid plugs the elbow and prevents the gas from entering the riser. It can also be deduced that the liquid has skewness around the lower elbow. This is mainly because the liquid falls back from the riser at a greater rate than for the feed pipe, due to the inclination. Gas accumulates in the top of the system and after approximately 124 seconds the gas is fully displaced from the riser pipe and pure liquid production occurs.

At approximately 248 seconds into the simulation a fully separation is obtained with the liquid in the riser pipe and lower part of the feed pipe and the gas in the top part of the feed pipe.

As gas and liquid is still fed to the system the gas will displace the liquid in the feed pipe until the gas pocket reaches the lower elbow. The gas will hereafter enter the riser at a fairly constant rate.

A high velocity, due to the unsuitable friction model for the riser pipe, causes a very low gas fraction. The system is therefore depicted again time step 400 seconds with a different scale in figure 9.3.

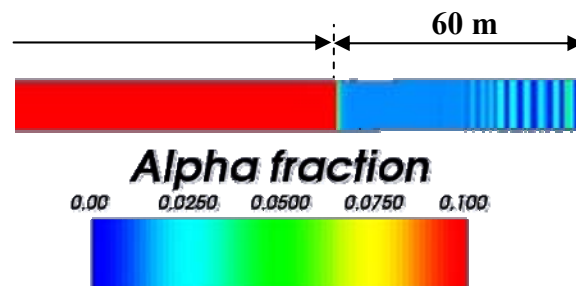


**Figure 9.3. Volumetric gas distribution for time step 400 seconds.**

It can be seen from 9.3 that the gas forms small slugs. This is however due to instabilities from the implemented friction model. There will be accounted for these instabilities later in the section.

The value of the volumetric gas fraction was logged through the `sampleDict` feature. The values were extracted by implementing a sample line with 560 points which logs the field of interest for each time step. The sample line was placed so it penetrated each cell. The values for the seven selected time steps are presented in figure 9.4.

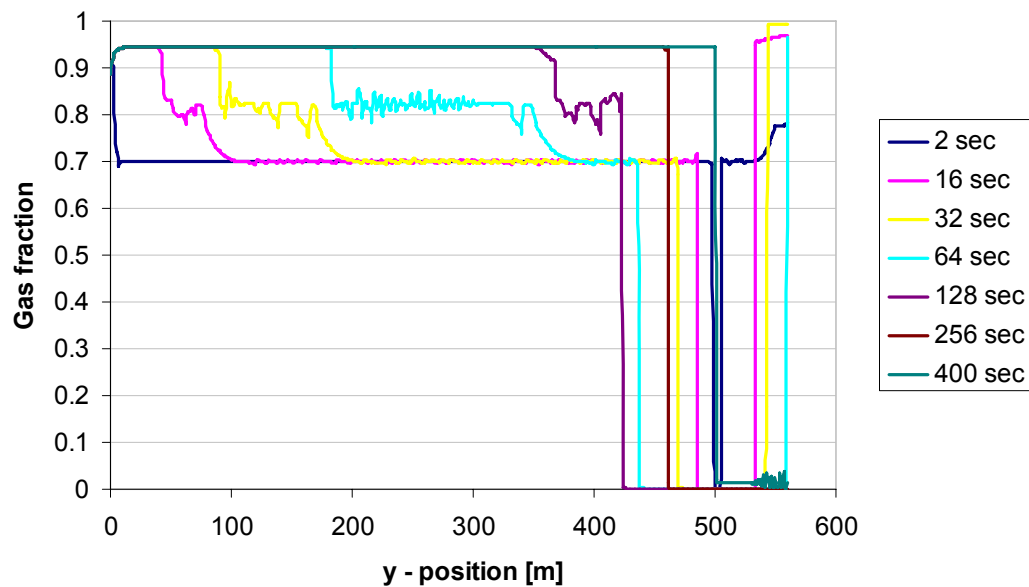


Figure 9.4. Values for volumetric gas fraction for seven selected time steps.

It can be seen from figure 9.4 that the maximum value for  $\alpha$  is approximately 0.95 in the feed pipe. This corresponds with the fact that liquid is fed to the feed pipe and the  $\alpha$  value can therefore not reach 1.

### Velocity distribution

The velocity distribution for the gas and liquid is presented by the `sampleDict` feature. Only the y-component of the velocity vector is extracted from the calculations as both the x- and z-component are zero. A negative velocity refers to a flow condition where the gas flows in the direction from the riser to the feed pipe. The gas velocity from the seven selected time steps is presented in figure 9.5.

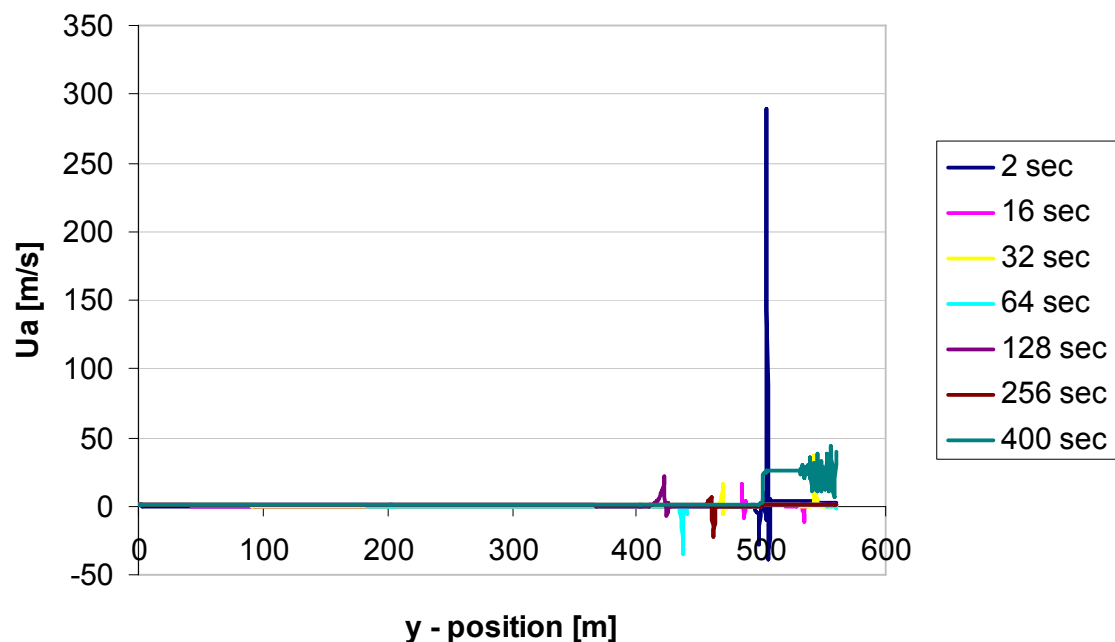
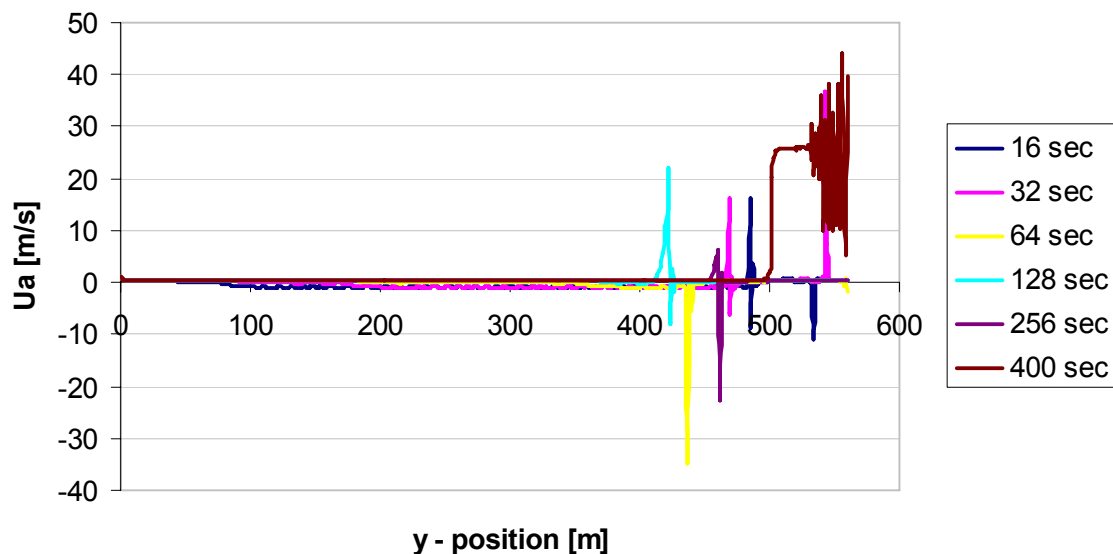


Figure 9.5. Gas velocity distribution.

It can be seen from figure 9.5 that the gas velocity exceeds 280 m/s. This extreme velocity occurs only in the start of the simulation and it is therefore assumed that it is caused by the liquid falling back from the riser. The extreme velocity occurs at the interface between the falling liquid and the rising gas. Consider the liquid falling back from the riser. The friction model assumes stratified flow for the liquid and it is therefore accelerated to a high velocity. This causes a rapid displacement of the gas which is accelerated to an extreme velocity at the interface. This is partly due to the high density difference between the liquid and gas, partly due to the low gas fraction at the interface. The gas velocity distribution without the initial gas velocity is presented in figure 9.6.



**Figure 9.6. Gas velocity distribution without initial time step.**

Figure 9.6 indicates that the gas velocity is accelerated to high velocities at the interfaces. This is due to the fact that the gas occurs at a small fraction which is accelerated by the liquid. As previously stated the friction model is only semi implicit and it utilizes an old value for the explicit part. This means that the gas can be momentarily accelerated to a high velocity, before the magnitude of the friction corresponds to the actual velocity. This phenomenon is exposed in figure 9.6.

Another interesting phenomenon is the oscillations of the gas velocity after 400 seconds. This is also assumed to be the result of the semi implicit friction model. The phenomenon is also presented in figure 9.7.

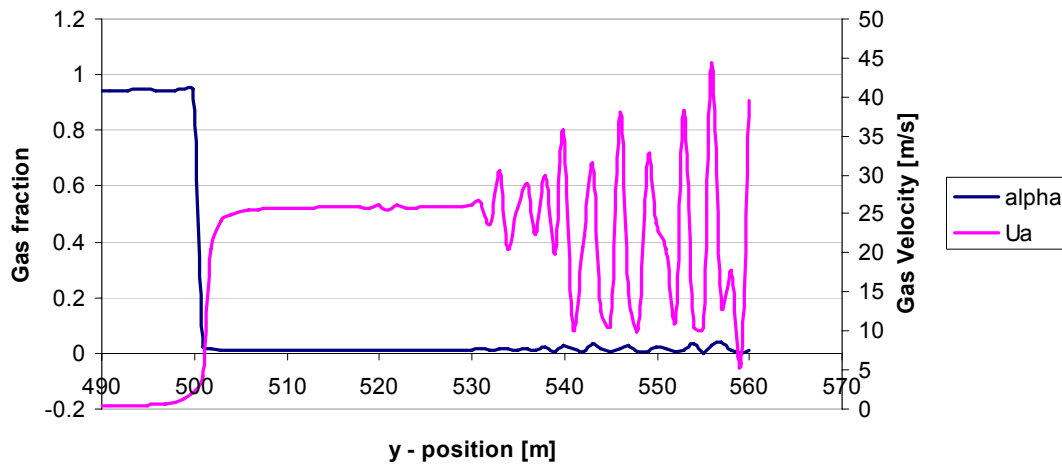


**Figure 9.7. Velocity and volumetric fraction for the gas at time step 400.**

It can be seen from figure 9.7 that the fluctuating velocity results in fluctuations in the gas fraction. The phenomenon can be explained by focusing at a specific node.

1. At time step  $x$  a small fluctuation is introduced, which result in an increased velocity. The friction term is only partly based on the new velocity.
2. At time step  $x+1$  the friction term is calculated based on the old velocity. This causes an increase in the magnitude of the friction term, which results in a lower velocity.
3. At time step  $x+2$  the friction term is calculated based in the previously calculated low velocity, which results in a low friction term and hence a high velocity.
4. The oscillations are assumed to grow until the calculation becomes unstable.

The velocity distribution for the liquid is presented in figure 9.8, represented by the seven selected time steps.

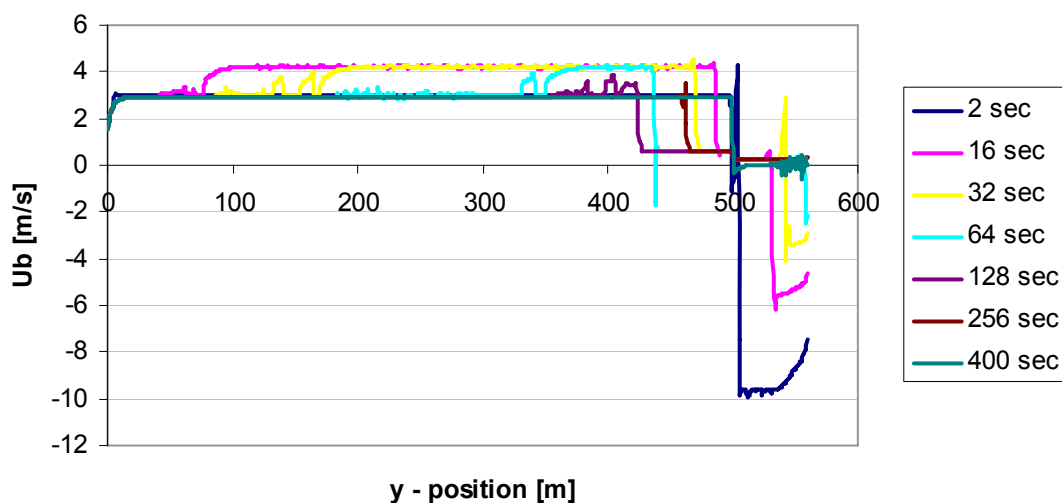


**Figure 9.8. Velocity distribution for the liquid.**

It can be seen from figure 9.8 that the liquid reaches a fairly high velocity as it falls back from the riser pipe. This can explain the violent acceleration of the low density gas due to

momentum transfer. It can also be seen that the velocity is fairly constant at the feed pipe ( $\sim 2.5$  m/s). The liquid reaches a higher velocity at the initial time steps because initial liquid distribution accumulates in the lower part of the system.

### Pressure distribution

The pressure distribution is extracted by the `sampleDict` feature. The outlet is set to 10 bars as previously stated. The pressure distribution for the seven selected time steps is presented in figure 9.9.

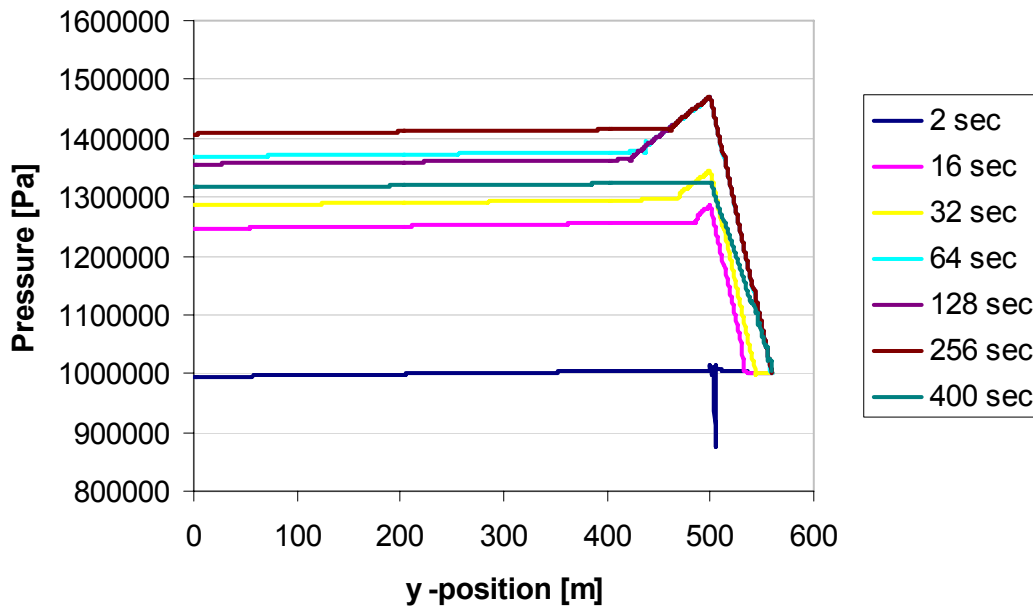


**Figure 9.9. Pressure distribution.**

It can be seen from figure 9.9 that a decrease in the pressure occurs at the initial time step. This is due to the acceleration of the gas previously described. The highest pressure obtained is at time steps 64, 128, 256, and 400 seconds. This corresponds to the time steps where the riser is fully filled with liquid. The highest inlet pressure is at time step 256 seconds, where the liquid level in the feed pipe is displaced by the gas. The pressure distribution is therefore in accordance with both the volume fraction and fluid velocity distribution.

## 9.2 Simulating unstable system

This section will present a simulation of an unstable pipe-riser system. The instability of the system is guaranteed by the equations presented in section 2.4 Stability Criterion. The analysis of the simulation is subdivided into

- Initial conditions
- Processing
- Results

### 9.2.1 Initial conditions

The pipe-riser system is illustrated in figure 9.10

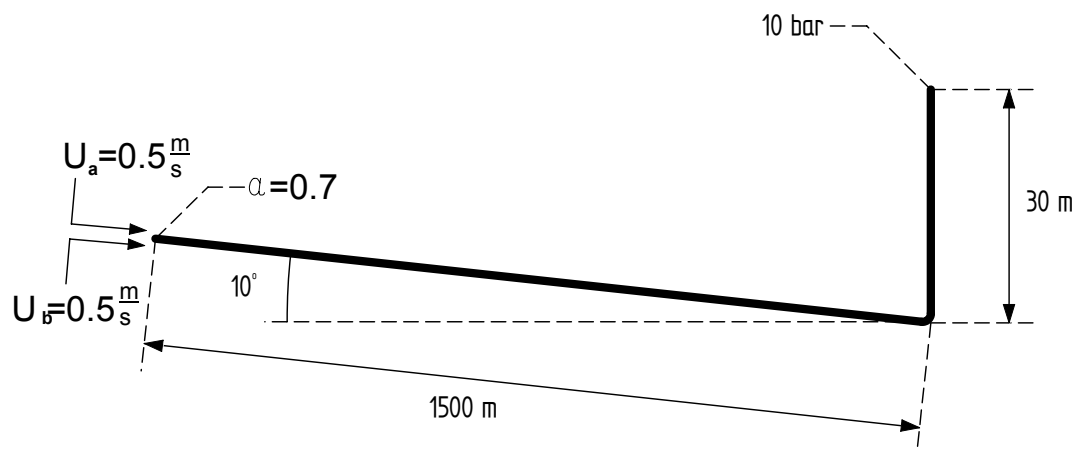


**Figure 9.10. Instable pipe-riser system**

The initial values and boundary conditions are the same as for the stable system.

### 9.2.2 Processing

The solver processed the instable case for a time domain of 1000 seconds with a write interval of 2 seconds. This resulted in a clocktime of 42866 seconds with an execution time of 32632 seconds. It should be noted that it was chosen to print the residuals to the screen during the processing. The PISO algorithm corrector was set to 2 and the alpha algorithm corrector was activated and the number of alpha correction loops was set to 2.

The above mentioned calculations conditions resulted in a very low courant number ( $\sim 0.02$ ) for the majority of the calculations.

### 9.2.3 Results

The results for the instable system are evaluated in same manner as for the stable system.

#### Volume fraction

The calculated time domain is represented by nine selected time steps, presented in figure 9.11. It is chosen to represent the analysis by 9 time steps ranging from 0 to 1060 seconds. After approximately 1060 seconds the system becomes stable.

## Simulation of pipe-riser system

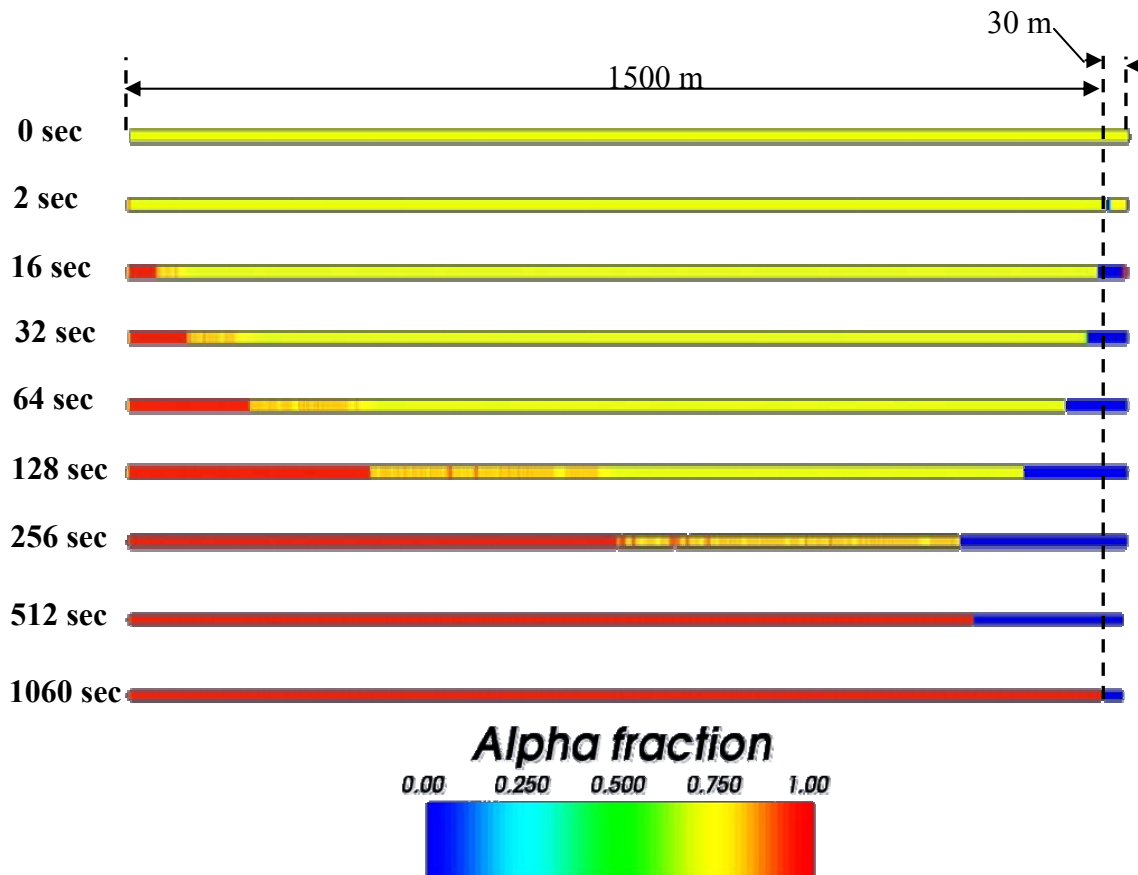


Figure 9.11. Volumetric gas distribution for unstable system. The 1500 m represents the 10° downward inclined feed pipe. The 30 m represents the vertical riser pipe. 0 refers to pure liquid and 1 refers to pure gas.

It can be seen from figure 9.11 that the gas and liquid distribution assumes same tendencies as for the stable system. The liquid accumulates in the lower section of the system and blocks the pipe. Gas is accumulated in the higher parts of the pipes. At approximately 512 seconds a fully separation is achieved. Gas and liquid is still fed to the system and the gas displaces the liquid in the feed pipe eventually. Hereafter is the gas fed to the riser pipe. A high velocity, due to the unsuitable friction model for the riser pipe, causes a very low gas fraction. The system is therefore depicted again time step 1060 seconds with a different scale in figure 9.12.

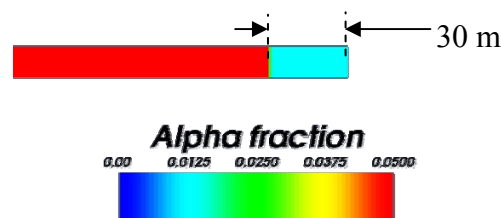
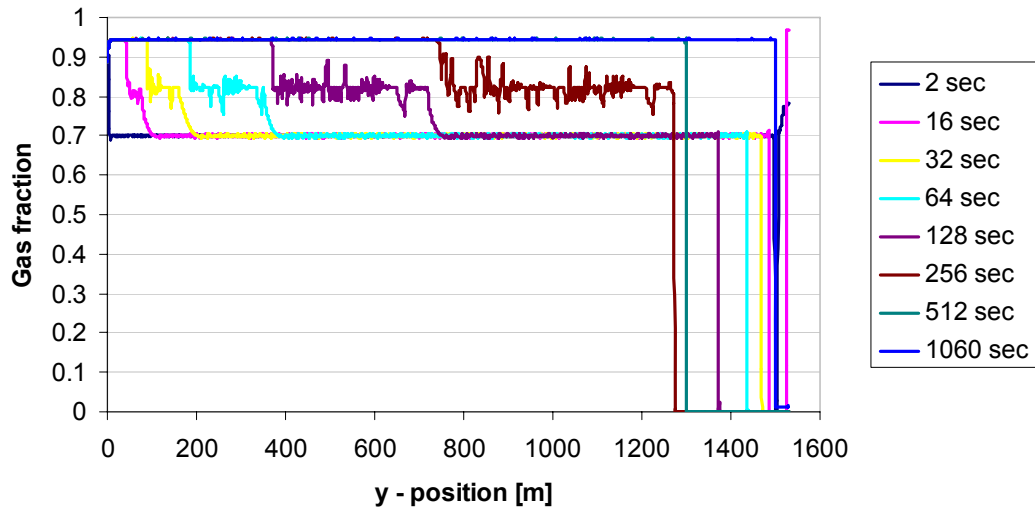


Figure 9.12. Volumetric gas distribution for time step 400 seconds.

The alpha fraction expressed graphically is presented in figure 9.13.



**Figure 9.13. Values for volumetric gas fraction for seven selected time steps.**

It can be seen from figure 9.13 that no severe slugging phenomenon is observed at the selected time steps. All additionally time steps were also investigated without severe slugging was observed. The results were similar to those for the stable system.

### Velocity distribution

The velocity distribution is again represented by the y-component of the velocity vector. A positive value refers to a flow direction from the feed pipe to the riser. A negative velocity value refers to a flow direction from the riser to the feed pipe. The gas velocity from eight selected time steps is presented in figure 9.14

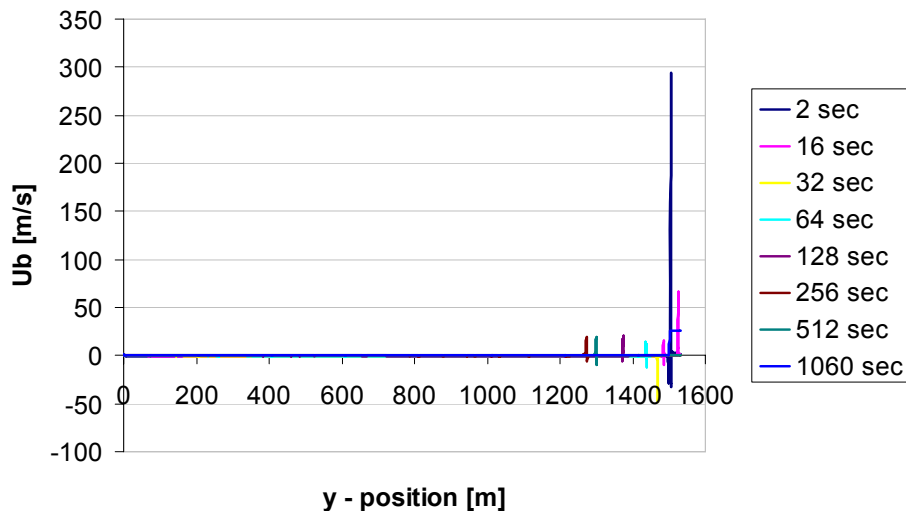


**Figure 9.14. Gas velocity distribution.**

As for the stable condition the gas velocity exceeds 280 m/s. The cause is the same as for the stable system. The gas velocity distribution without the initial time step is presented in figure 9.15.



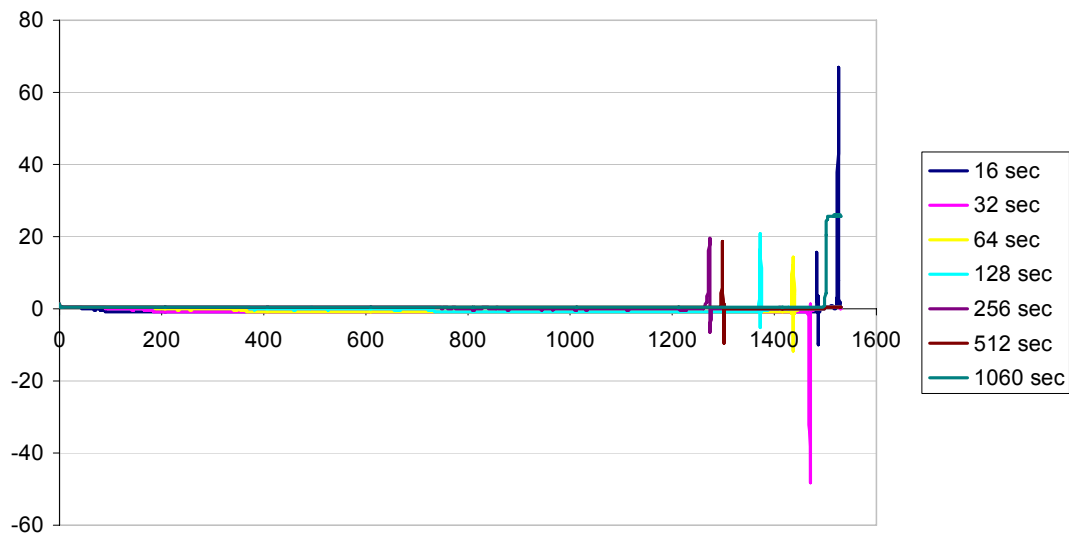


**Figure 9.15. Gas velocity distribution without initial time step.**

Again, the velocity distribution is similar as for the stable system. The gas velocity is, however, stable in the riser for the last time step. This is most likely because the riser height is shorter. The instability occurs after approximately 40 meters for the stable system.

The velocity distribution for the liquid is presented in figure 9.16.

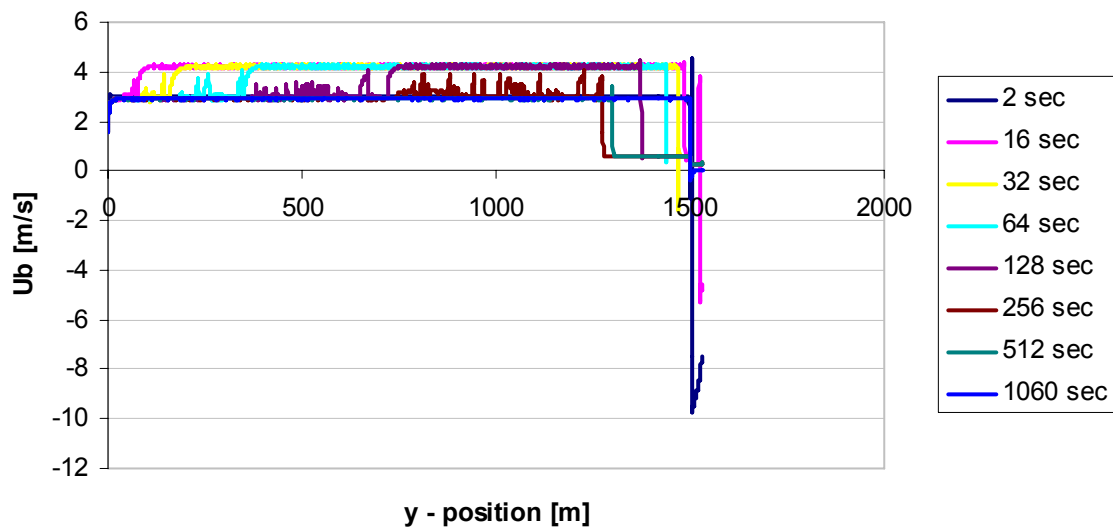


**Figure 9.16. Velocity distribution for the liquid.**

The liquid velocity is similar to the results from the stable conditions and no severe slugging is observed.

### Pressure distribution

The pressure distribution is presented in figure 9.17.

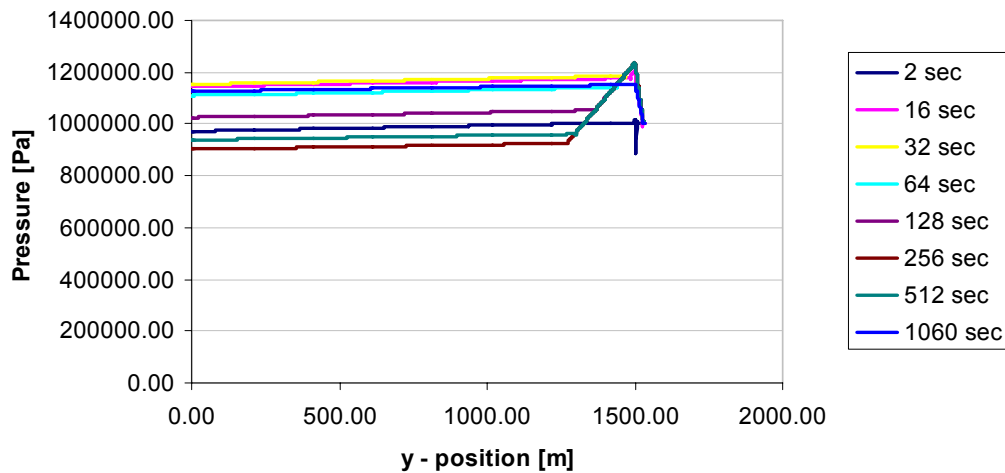


**Figure 9.17. Pressure distribution.**

Again, the pressure is similar to the results from the system with stable conditions. No severe slugging is observed.

### 9.3 Summary of results

It can be concluded from the simulations that the model was incapable of simulating severe slugging. The system with unstable boundary conditions achieved results similar to system with stable conditions. This can mainly be due to two reasons; friction and compressibility.

The friction model is unable to keep the gas velocity at moderate velocities in the riser. The high velocity results in a low alpha fraction. The low alpha fraction does not lower the riser mixture density sufficiently and thereby the static pressure. This prevents a blow out situation by the gas.

Another reason could be due to the lack of gas compressibility. The incompressible gas is not able to create the driving pressure which occurs at severe slugging. Furthermore will the incompressible gas not expand in the riser and it will therefore not cause an additional decrease in static pressure.

The enclosed cd-rom includes frequencies of the two simulations. In addition are all simulation data also to be found on the cd-rom.

## 10 Discussion

In this section issues related to the current project are discussed. The section is divided into three sections;

- Refinement of friction model
- Implementation of compressibility
- Future work

Refinement of friction model is proposals of methods to improve the friction model for the one dimensional solver.

Implementation of compressibility is related to the incorporation of a compressibility model into the one dimensional solver.

Future work proposals are given both with regard for the existing model, but also with regard to additional opportunities for the model after small modifications.

### 10.1 Refinement of friction model

There are two governing shortcomings in the friction model incorporated. The first is based on a CFD-technical assumption and the other is due to the empirical friction model utilized.

The CFD-technical shortcoming is caused by the fact that the magnitude of the friction is partly based on an old velocity value. This can rather easily be avoided by implementing the source term as fully implicit.

The shortcoming due to the empirical friction model utilized is, however, more comprehensive. A one-dimensional model is not capable to distinguish between the different flow regimes and is thereby unable to determine the appropriate friction model to the flow. Implementation of a deterministic model is an option, where a mechanistic model could determine the flow pattern. An appropriate friction model could hereafter be applied to each node and a more correct momentum equation would be obtained.

### 10.2 Implementation of compressibility

Several attempts to implement compressibility in the model were tried during the project period. The compressibility of the gas was implemented using an ideal gas model, while the liquid was still assumed incompressible. A modified continuity equation was the basis for a new deduction, which resulted in a modified alpha equation and pressure equation. The model was able to compile and initiate the calculations. However, the model became unstable approximately 1 second into the time domain. Numerous attempts were made to make the model stable, but without success.

It is assumed unrealistic to simulate severe slugging without a compression of the gas, because the driving force which causes the severe slugging is due to the expansion of the gas.

## 10.3 Future work

Suggestions for future work are given below.

- Deterministic model for flow regime prediction
- Compression of the gas
- Simulation of hydrodynamic slugging
- Simulation of severe slugging prevention

Short explanations of the above listed proposals are given in the following.

### 10.3.1 Deterministic model for flow regime prediction

Several mechanistic models are developed to determine flow patterns. These models are often validated through experimental work and several are even validated with actual field data. Several mechanistic semi-empirical friction models are also developed and validated. They are often relatively simple and require no iterations. The model should be implemented by extending the friction model already implemented.

### 10.3.2 Compression of the gas

Recently, a new compressible two phase solver is released with OpenFOAM-1.5, denoted `compressibleInterFoam`. Modifying this solver or implementing the compressible terms in the `1DslugFoam` solver would be obvious.

### 10.3.3 Simulation of hydrodynamic slugging

Many efforts have been made to simulate hydrodynamic slugging. By implementing Kelvin-Helmholtz theory in the `1DslugFOAM` it should be able to simulate this phenomenon. The model should not only be able to predict hydro dynamic slugging, but it should also be able to predict slug flow factors. This does, however, require improved friction and mixing models for the solver.

### 10.3.4 Simulation of severe slugging

It could be advantageous to investigate the impact on severe slugging from process equipment, especially from process equipment implemented to prevent severe slugging. Increased back pressure can simply be investigated by increasing the outlet pressure. The impact from gas injection and choking is more comprehensive.

Gas injection could be simulated by dividing the model into two domains; one upstream the injection point and one downstream the injection point. The inlet value of the alpha fraction for the downstream domain should then be the sum of the outlet value for the upstream domain and the gas injected. This fraction should then be normalized with respect to the amount of injected gas.

Choking can be simulated by implementing an additional pressure term. This pressure term should simulate the effect from the choking valve by making it depend on the velocity.

Above proposals for future work are simply suggestion based on the present project work. It is not dismissed that more efficient and appropriate solution to the future work exists.

# 11 Conclusion

The primary objective for this project has been to develop a solver capable of simulating severe slugging. As it is too comprehensive to develop a fully functional solver it was chosen to focus on the framework for the solver and hereafter validate the general approach for a one-dimensional model.

The model was developed in the open source program OpenFOAM. The solver, denoted 1DslugFoam was created and associated case directories were created.

The governing theory and algorithm for the one dimensional model was based on conditional averaging and the PISO algorithm. An empirical based friction model was implemented and the pipe inclination was incorporated by setting the gravitational acceleration as a variable vector field. These features were tested in order to ensure that the governing physical behavior was captured by the model.

The OpenFOAM coding for the solver and case structure was presented and the link between the coding and theory was established.

Two tests were performed to validate the solver; a test where the physical conditions would ensure a stable flow and a test where the conditions would ensure severe slugging.

Both cases, however, illustrated stable systems, which indicated that the solver was unable to simulate severe slugging. The friction model incorporated resulted in numerical instabilities due to the semi-implicit form in the momentum equation and the friction model was inappropriate at describing the flow in the riser.

To summarize; a two-phase one-dimensional solver in preparation for simulating severe slugging was developed. The solver was capable to capture physical behavior such as friction, static pressure and buoyancy. The solver was documented and suggestions for improvement, refinement, and future work was proposed.

# References

- 1 Dodd, J., Ed.; "The ACS Style Guide, a manual for authors and editors," 2nd ed.; ACS: Washington, 1997
- 2 Taitel Y.: "Stability of Severe Slugging," International Journal of Multiphase flow, Vol. 12, No. 2, pp. 203-217 (1986)
- 3 Bøe, A.: "Severe Slugging Characteristics", Selected Topics in Two-Phase flow, NTH, Trondheim (1981)
- 4 Nicklin, D. J. and Davidson J. F.: "The Onset of Instability on Two Phase Slug Flow," Inst. Mech Engr. Proc. of Symp. On Two Phase Flow, Paper No. 4 (1962)
- 5 Harmathy, T.Z.: "Velocity of Large Drops and Bubbles in Media of Infinite or Restricted Extent," AIChE Journal, Volume 6, pp. 281 (1960)
- 6 Weller H.G.: "Derivation, Modelling and Solution of the Conditionally Averaged Two-Phase Flow Equations," Technical report, Nabla Ltd. (2005)
- 7 Dopazo C.: "On Conditional Averages for Intermittent turbulent flows," Journal of Fluid Mechanics, Vol. 81, No. 3, pp. 433-438 (1977)
- 8 Weller H.G.: "The Development of a New Flame Area Combustion Model Using conditional averaging," Thermo-Fluids Section Report TF 9307, Imperial College of Science, Technology and Medicine (1993)
- 9 C. T. Crowe et al.: "Numerical Methods in Multiphase Flows" ASME Fluids Engineering Division, USA, volume 185, (1994)
- 10 OpenFOAM User Guide, v 1.4.1. 2007. © 2000-2008 OpenCFD Ltd.
- 11 OpenFOAM Programmes Guide, v 1.4.1. 2007. © 2000-2008 OpenCFD Ltd.
- 12 Taitel Y. and Dukler A. E.: "A Model for Predicting Flow regime Transitions in Horizontal and Near Horizontal Gas-Liquid Flow," AIChE Journal 22, No. 1, pp. 47-55 (1976)
- 13 Kokal, S. L. and Stanislav J. F.: "An Experimental Study of Two-Phase Flow in Slightly Inclined Pipes-I. Flow Patterns," Chemical Engineering Science, Vol.44, No.3, pp. 665-679 (1988)
- 14 Dukler, A. E. and Hubbard, M. G.: "A Model for Gas-Liquid Slug Flow in Horizontal and Near Horizontal tubes," Ind. Engng Chem. Fundam. Vol. 14, pp. 337-347 (1975)
- 15 Taitel Y., Barnea D. and Dukler A.E, "Modelling Flow Pattern Transitions for Steady Upward Gas-Liquid Flow in Vertical Tubes," AIChE Journal, Volume 26, pp. 345-354 (1980)
- 16 Barnea D., Shoham O., Taitel Y., "Flow Pattern Transition for Vertical Downward Two Phase Flow," Chemical Engineering Science, Volume 37, No. 5, pp. 741-744 (1982)
- 17 Crawford T.J., Weinberger C.B., Weisman J., "Two Phase Flow Patterns and Void Fractions in Downward Flow Part I: Steady State Flow Patterns," International Journal of Multiphase flow, Vol. 11, No.6, pp. 761-782 (1985)
- 18 Nicklin D.J and Davidson J.F., "The Onset of Instability on Two Phase Slug Flow," Inst. Mech. Engr., Proc. of Symp. on Two Phase Flow, Paper 4 (1962)
- 19 Griffith P. and Wallis G.B., "Two Phase Slug Flow," Journal of Heat Transfer, Vol. 83 pp. 307 (1961)

## References

---

- 20 Barnea D., "A Unified Model for Predicting Flow Pattern Transitions for the Whole Range of Pipe Inclinations," International Journal of Multiphase flow, Vol. 13, No.1, pp. 1-12 (1987)

## Appendix A Flow patterns

In order to utilize and understand the mechanistic models it is vital to understand the basic flow patterns and the general mechanisms which trigger a transition between the flow patterns.

This problem analysis will go through the flow patterns which characterize the distribution of the phases in the pipe. It will clarify the transition effects that are dominant when the distribution changes from one pattern to another. Finally an attempt to clarify other basic factors which can affect the flow pattern is carried out.

Two phase flow is well understood and fairly accurate mechanistic models are developed for this compared to three phase flow. This problem analysis will only treat two phase flow problems, since three phase flow is still not understood. A reasonable accuracy can, however, be obtained by applying two phase models to three phase flow. Two-phase flow refers to the transportation of liquid and natural gas, in this case transportation of oil and gas. Three phase flow refers to the transportation of oil, water, and natural gas.

Due to gravitational forces one has to consider the pipe inclination. The transition mechanics for horizontal flow differs significantly from inclined and vertical, due to simplification of the physical phenomena. Even small inclination changes affect the transition greatly. Therefore it is necessary to distinguish between the following;

- Horizontal pipes
- Vertical pipes
- Inclined pipes

A description of the flow patterns and the mechanisms which triggers flow pattern transition for the above listed inclinations is carried out in the following.

### A.1.1 Horizontal pipes – Flow patterns

The change from one pattern to another is a gradual transition and through these transition phases the pattern will possess properties from both patterns. This means that the transition will be exposed to some subjective perception. The flow distribution can therefore be divided into numerous patterns. A systematic and general dividing is therefore needed in order to determine the main principles of the distribution for further simulations of the patterns. The distributions for the transporting fluids in horizontal pipes have been classified in four major flow patterns listed below;

- Stratified flow
- Intermittent flow
- Annular flow
- Dispersed bubble flow

Taitel & Dukler<sup>12</sup> presented a model where the above four flow patterns were further subdivided and a mechanistic model was proposed. The following classification is based on their work. They suggested a flow pattern map based on the superficial velocities. The flow pattern map is presented in figure 11.1 with the general outline for the transition zones.

---

<sup>12</sup> Taitel & Dukler (1976), "A Model for Predicting Flow regime Transitions..."



## Appendix A

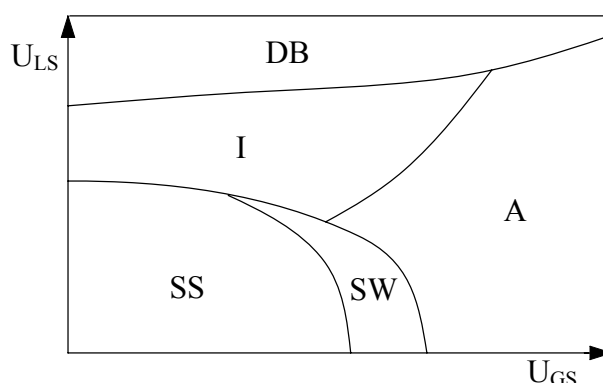


**Figure 11.1.** Flow pattern map for horizontal flow presented by Taitel and Dukler, 1976. Stratified Smooth (SS), Stratified Wavy (SW), Intermittent (I), Annular (A), Dispersed Bubble (DB).  $U_{LS}$  is the superficial liquid velocity and  $U_{GS}$  is the superficial gas velocity.

The flow pattern map above is not general but only valid for one certain scenario. It will depend on diameter, fluid characteristics, and operating values. Figure 11.1 presents only one of many flow pattern maps. Other flow pattern maps can be based on dimensionless values.

### Stratified flow

Stratified flow refers to a distribution where the liquid flows at the bottom of the pipe and the gas flows at the top of the pipe. At this regime there is no mixing between the two phases and the interface is smooth. This regime is denoted Stratified Smooth (SS). With an increase in the gas flowrate the interface will become wavy, and will have a rough appearance

. Small bubbles can also be observed at the liquid surface<sup>13</sup>. This regime is denoted Stratified Wavy (SW). The two regimes are illustrated in figure 11.2 and 11.3. The velocity of the gas is greater than the velocity of the liquid.

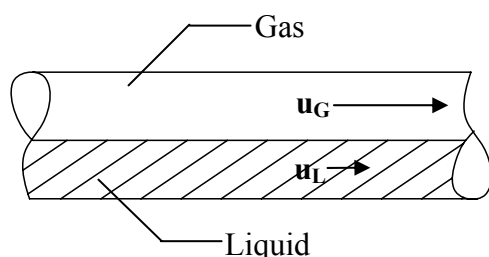


**Figure 11.2.** Stratified Smooth (SS) flow pattern.

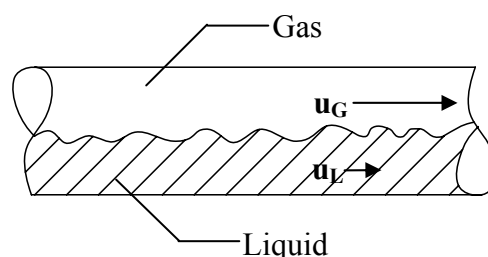


**Figure 11.3.** Stratified Wavy (SW) flow pattern.

The vital geometric parameters of the stratified flow are presented in figure 11.4. All parameters depend on the liquid height  $h_L$ .

<sup>13</sup> Kokal & Stanislav (1988), "An Experimental Study of Two-phase Flow..."

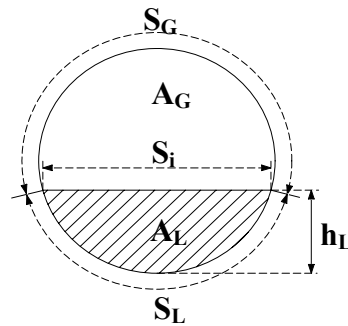


Figure 11.4. The geometry of a stratified flow.

### Intermittent flow

Intermittent flow refers to a distribution of the fluids where the flows in alternating packages of mainly gas and mainly liquid. One can also regard it as a liquid slug with entrained gas, a gas bubble and a liquid film. Since the governing effects vary over the length of the slug, Dukler & Hubbard<sup>14</sup> suggested that the total slug length is divided into four subdivisions. The subdivisions are; mixing zone, liquid slug body, slug tail, and liquid film. These zones are illustrated in figure 11.5.

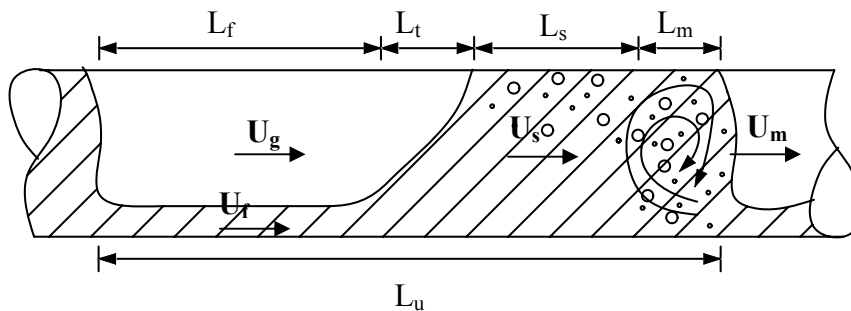


Figure 11.5. The four basic zones of the intermittent slug.  $L_m$  refers to mixing zone,  $L_s$  to liquid slug body,  $L_t$  to the slug tail, and  $L_f$  to the liquid film.

The mixing zone is where the liquid film in front of the slug is scooped up. Due to the difference in kinetic energy the film will penetrate a distance into to the slug, before reaching the slug velocity. This creates an eddy at the front of the slug which also can be regarded as a mixing vortex. Due to the violent mixing a great amount of gas is entrained in this zone.

The liquid slug body is the main part of the slug. The length is normally several pipe diameters. Some gas is entrained in the slug, due to the mixing vortex. The slug body will grow in length until a balance between shedding at the tail and scooping up in the mixing zone is reached. A normal stable liquid slug length is approximately  $30D$ , but can vary significantly in length.

At the slug tail liquid is shed of from the slug body. The liquid height varies significantly in this region due to the shedding. The liquid which is shed of experiences a decrease in velocity and forms a thin layer of liquid film. Just after shedding the velocity of the liquid rapidly decreases, until it assumes a fairly constant velocity before being swept up by the following slug. One can

<sup>14</sup> Dukler, A. E. & Hubbard, M. G. (1975), "A model for gas-liquid slug flow..."

## Appendix A

therefore regard a stable liquid slug as a phenomenon where the amount of shedding is equal to the amount of liquid swept up from the preceding slug.

The intermittent flow regime can be subdivided into four separate classifications; Elongated bubble (EB), Elongated bubble with dispersed bubbles (EDB), Slug (SL), and Slug froth (SLF). The classification of this depends on the gas entrained in the liquid slug. The four sub-patterns are illustrated in 11.6.

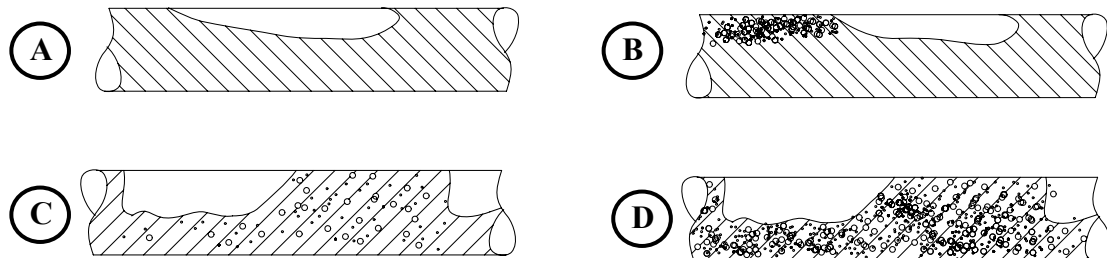


**Figure 11.6. The four sub-patterns. A: Elongated bubble (EB), B: Elongated bubble with dispersed bubbles (EDB), C: Slug (SL), D: Slug froth (SLF).**

Elongated bubble is a distribution where the liquid slug body is free of entrained gas and flows in a laminar regime. The gas bubble is long and streamlined and the interface between the phases is stratified. The tail of the gas tends to break off from the main bubble, and is subsequently swept up by the following main bubble.

Elongated bubble is a distribution where the slug body contains gas bubbles. As the velocity increases, the slug body flow regime changes to turbulent. A mixing zone is created between the tail of the gas and the nose of the slug, due to the turbulent forces.

Slug is a regime distribution where the interface between the main gas bubble and the film becomes similar to the gas-liquid interface for SW.

Slug froth refers to a distribution where a great amount of gas is entrained in the liquid. Due to the turbulent fluctuations intermixing occurs and the slug body and liquid film becomes frothy due to the entrained gas.

### Annular flow

Annular flow refers to a distribution where the gas flows in an inner-core and the liquid forms a film layer on the pipe wall, surrounding the gas core. At low gas velocities the liquid film will mainly gather at the bottom half of the pipe, this regime is denoted Annular Wall (AW). At higher gas velocities liquid is shed from the film layer and entrained as droplets into the gas core. A thin layer of liquid film will surround the gas core and a balance between droplets coalescing at the wall and shedding will be obtained. This regime is denoted Annular Mist (AM).

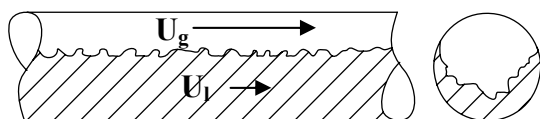


**Figure 11.7. Annular wall pattern (AW). To the right is a cross sectional view presented.**

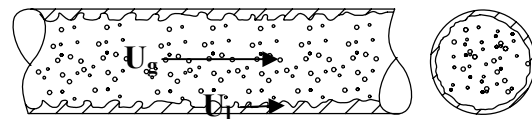


**Figure 11.8. Annular mist pattern (AM). To the right is a cross sectional view presented.**

### Dispersed bubble flow

Dispersed bubble flow refers to a distribution where all gas is entrained in the liquid. At low flowrates bubbles will gather at the top section of the pipe due to buoyancy, and at higher flowrates the bubbles are uniformly distributed in the liquid. This regime is denoted Dispersed Bubble (DB). At higher flowrates the intermixing can become so strong that the liquid becomes frothy. This regime is denoted Dispersed Froth (DBF), but is also commonly referred to as Churn.

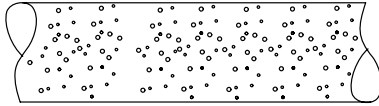


Figure 11.9. Dispersed bubble pattern.

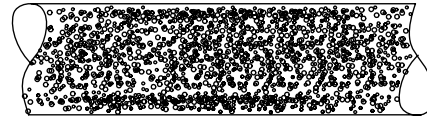


Figure 11.10. Dispersed Froth pattern.

### A.1.2 Horizontal pipes – Transitions

The triggering effect for transition between flow patterns is a complex matter, where several opposite acting mechanisms are factors. This section will describe the basic functions which takes place at a transition phase between the regimes. The transitions between flow regimes are listed below;

- |  |   |                   |
|--|---|-------------------|
| • From stratified smooth to stratified wavy      | – | SS-SW transition  |
| • From stratified to non-stratified flow         | – | S-I/A transition. |
| • From intermittent to dispersed bubble flow     | – | I-DB transition   |
| • From intermittent to annular flow              | – | I-A transition    |
| • Elongated bubble to elongated dispersed bubble | – | EB-EDB transition |
| • Elongated dispersed bubble to slug flow        | – | EDB-SL transition |
| • Slug to slug froth flow                        | – | SL-SLF transition |

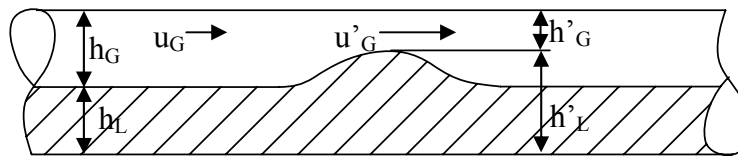
#### SS-SW transition

The SS-SW transition is due to the interfacial shear between the gas and the liquid. When the velocity difference between the phases becomes sufficient, the slip effect will create small waves at the interface.

#### S-I/A transition

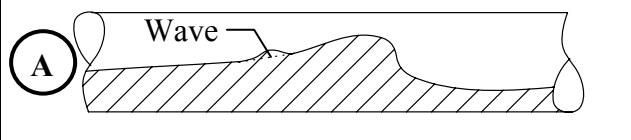
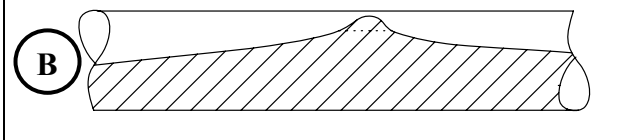
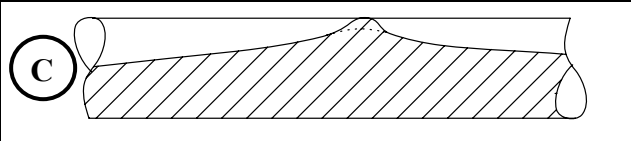
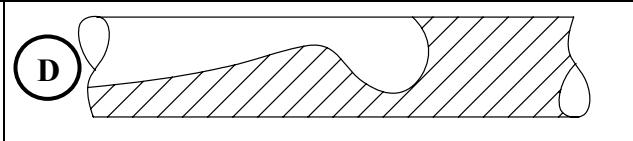
The transition from stratified to non-stratified flow can evolve to either intermittent flow or annular flow. Intermittent flow will occur if the liquid fraction is large enough. If inadequate, annular flow will occur. It is the same mechanism which is dominating from stratified to intermittent flow as in stratified to annular flow. The transition from stratified to non-stratified is mainly determined by two opposite acting forces; gravity and the Bernoulli Effect. Consider a stratified flow where a wave is initiated at the interface. The cross sectional area occupied by the gas decreases due to change in liquid height caused by the wave. This causes the gas to accelerate over the wave and due to the Bernoulli Effect, a decrease in the gas-pressure occurs. This tends to make the wave grow.

## Appendix A



**Figure 11.11. The change in liquid height causes a higher gas flowrate over the wave.**

The gravity acts upon the wave and tends to make the wave decay. Thus, a transition from stratified flow will occur when the decrease in gas pressure is sufficiently large to overcome the flattening effect due to gravity. As the wave grows slugs will occur. This is illustrated in figure 11.12.

	
<p><b>A: A small wave appears.</b></p>	<p><b>B: As the sum of the liquid height and the wave reaches the top of the pipe, bridging occurs.</b></p>
	
<p><b>C: As bridging occurs, the high-velocity gas rapidly accelerates the liquid to the gas velocity.</b></p>	<p><b>D: As the liquid rapidly accelerates it scoops up the liquid in front and becomes a stable slug.</b></p>

**Figure 11.12. Above figures A-D illustrates the initiation of slug.**

### I-DB transition

The transition from intermittent to dispersed bubble flow is determined mainly by two opposite acting forces, buoyancy and turbulent forces. As the liquid flowrate increases, turbulent fluctuations will seek to shear the large elongated bubbles into smaller spherical bubbles. These small bubbles will be distributed reasonable uniformly in the liquid. Buoyant forces will tend to drive the bubbles to the top where they will coalesce. A transition will occur when the turbulent fluctuations are strong enough to overcome the buoyant forces.

### I-A transition

The transition from intermittent to annular flow depends on the liquid fraction in the pipe. As the gas flowrate increases at an intermittent flow, the liquid film will comprise a higher proportion of the liquid in the pipe. The gas pocket will eventually break trough the liquid slug body and annular flow will be obtained.

### EB-EDB transition

As the liquid slug flow changes from laminar to turbulent flow, small gas bubbles will due to turbulent fluctuations be entrained in the liquid slug. It is mainly gas from the gas tail that becomes entrained.

### EDB-SL transition

As the flowrate increases, the turbulent force increases. This result in a larger proportion of gas entrained in the liquid.

### SL-SLF transition

As the flowrate increases further a strong intermixing between the two phases will occur. A large proportion of the gas becomes entrained in the liquid. Due to the strong turbulent fluctuations in the liquid, spherical gas bubbles become uniformly distributed in the liquid.

### A.1.3 Vertical Pipes – Flow patterns

The distributions for the transporting fluids in vertical pipes have been classified in four major flow patterns listed below;

- Bubble flow
- Dispersed bubble flow
- Intermittent flow
- Annular flow

Even though the above flow patterns posses' similarities from the horizontal flow pattern, there are great differences in the governing transition mechanisms and flow parameters. The change from one pattern to another is a gradual transition and in these transition phases the pattern will possess properties from both patterns, as with horizontal flow. Taitel et al<sup>15</sup> presented a model where the flow patterns where categorized and the dominant transition factors were determined.

One must differ between vertical upward flow and vertical downward flow. The flow patterns have different characteristics and the transitions are triggered by different mechanisms, depending on whether it is upwards or downwards flow.

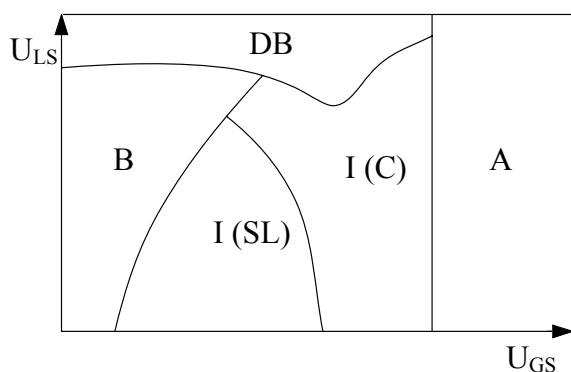


Figure 11.13. Flow pattern map for upwards vertical flow

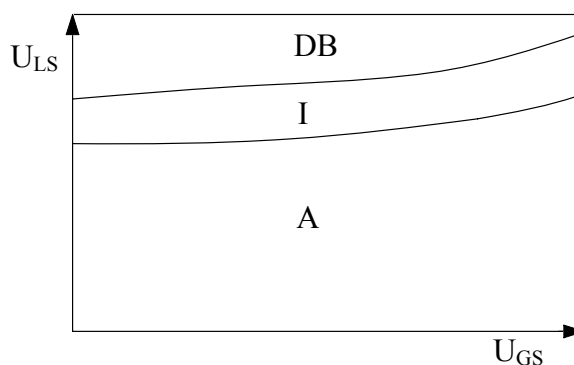


Figure 11.14. Flow pattern map for downward vertical flow<sup>16</sup>

Bubble (B), Slug (SL), Intermittent (I), Churn (C), Dispersed bubble (DB), Annular (A).

### Bubble flow

Bubble flow (B) refers to a distribution where the liquid is the continuous phase with bubbles of gas entrained. The size and shape of the bubbles is small stable spherical bubbles and larger wobbly bubbles. Above a critical bubble diameter, bubbles becomes deform and wobbly. The

<sup>15</sup> Taitel, Y., Barnea, D. & Dukler, A.E (1980), "Modelling flow pattern transitions for steady upward..."

<sup>16</sup> Barnea D., Shoham O., Taitel Y. (1982), "Flow pattern transition for vertical downward two phase flow"

## Appendix A

larger wobbly bubbles flow in a zigzag path and not in a rectilinear path as the small spherical bubbles. The bubble flow pattern is illustrated in figure 11.15.

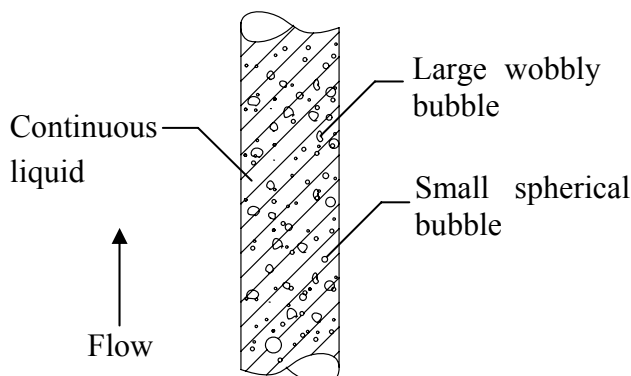


**Figure 11.15. Upward vertical bubble flow**

This flow pattern exists only for upward flow and not for downward flow. At downward flow the liquid will flow at the pipe wall, even at low liquid flowrate resulting in an annular flow instead of bubble flow.

### Dispersed bubble flow

As for horizontal flow, dispersed bubble flow (DB) is a distribution where the gas is uniformly distributed in the liquid as small spherical bubbles. The buoyant effect on the gas bubbles is neglectable, so it is assumed that the mixture is a homogenous mixture. The dispersed bubble flow is illustrated in figure 11.16.

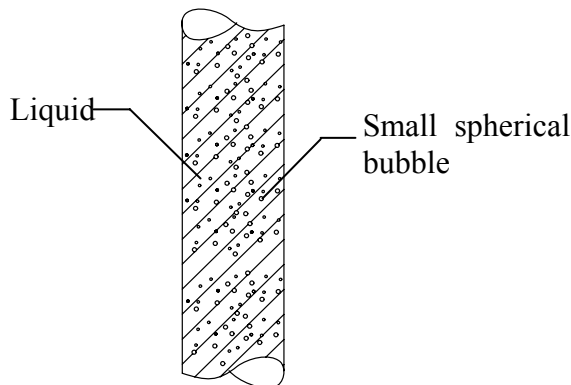


**Figure 11.16. Dispersed bubble flow**

### Intermittent flow

Intermittent flow refers to a distribution where the fluids flow in alternating packages of gas and liquid. The intermittent flow can be divided into slug and churn. Slug is a regime where the main gas part flows as Taylor bubbles separated by liquid which bridges the pipe. The Taylor bubble almost fills the cross sectional area of the pipe and the length is 1-2 diameters. The liquid bridge contains some entrained gas.

The slug flow is illustrated in figure 11.17 and 11.18.

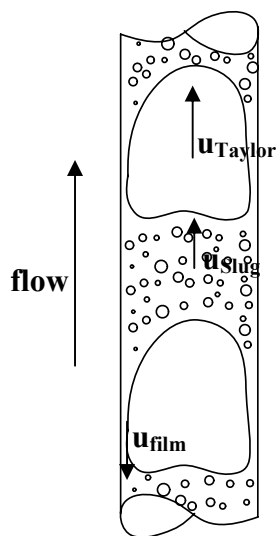


**Figure 11.17. The upward flowing slug pattern. Notice that the film is flowing downwards.**

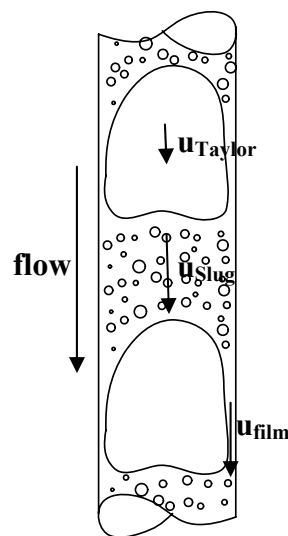


**Figure 11.18. The downward flowing slug pattern.**

For the upward flowing distribution the velocity of the Taylor bubble is higher than the velocity of the liquid slug. The liquid film at the wall is flowing downwards.

For the downward flowing distribution the velocity of the Taylor bubble is lower than the slug velocity. The Taylor bubble is moving upward with respect to the liquid. However, drag and viscous forces are always sufficient to give a net downward velocity.

Churn is similar to slug but behaves more chaotic and frothy. The large bubbles become narrower and lose their hemispherical shape. The liquid bridge continuity is repeatedly destroyed due to high local gas concentrations which make the liquid bridge collapse and fall before being accumulated and lifted by the gas.

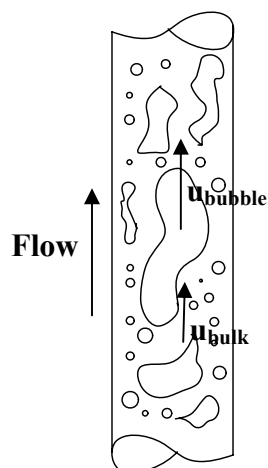


**Figure 11.19. The upward flowing churn pattern.**

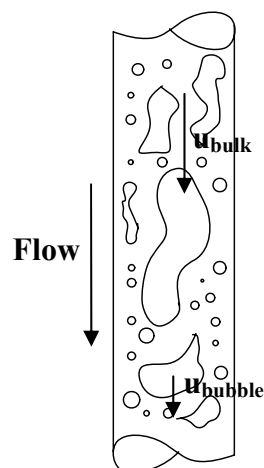


**Figure 11.20. The downward flowing churn pattern.**

For the upward flowing pattern the bubble velocity will be greater than the liquid bulk velocity. For downward flowing patterns the net bubble velocity is smaller.

## Annular flow



## Appendix A

Annular flow refers to a distribution where the gas flows in an inner-core and the liquid forms a film layer on the pipe wall, as for horizontal flow. Annular wall (AW) can not be obtained for vertical flow, only annular mist (AM).

For downward flow a distribution similar to annular flow can occur denoted Falling Film (FF)<sup>17</sup>. The difference between the flow patterns is that small droplets are entrained in the gas core for annular flow, while for falling film all liquid flows at the pipe wall. Falling Film is a specific case, which is unlikely to experience under field conditions and is therefore not treated further in this project.

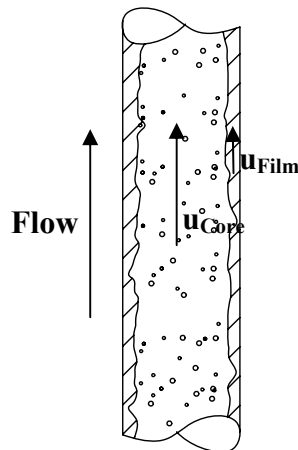


Figure 11.21. The upward flowing annular pattern. Notice that the film is flowing upwards.

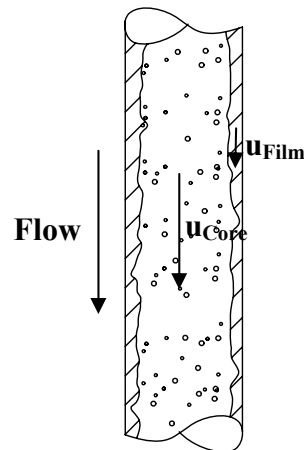


Figure 11.22. The downward flowing annular pattern.

### A.1.4 Vertical Pipes – Transitions

The governing transition mechanisms for vertical flow vary significantly from the triggering mechanisms for horizontal flow. This section will outline the basic mechanisms which act when transition in vertical flow occurs. The transitions between flow regimes are listed below;

- |   |                     |
|---|---------------------|
| • From bubble to slug flow                    | – B-SL transition   |
| • From bubble to dispersed bubble flow        | – B-DB transition   |
| • From dispersed bubble to slug flow          | – DB-SL transition  |
| • From slug to churn flow                     | – SL-C transition   |
| • From dispersed bubble/churn to annular flow | – DB/C-A transition |

#### B-SL transition

In the bubble flow bubbles randomly collide and coalesce, but the formed bubbles are also sheared due to turbulent fluctuations. As the gas flowrates increases the coalescence rate increases due to the higher concentration of gas bubbles.

For upward flow the bubbles will obtain a higher velocity when they coalesce due to the increased buoyant force compared to the drag and viscous forces. Due to the velocity increase and since the larger bubbles travels in a zigzag pattern they collide more often, which results in the self-perpetuating effect. Eventually gas travels as large Taylor bubbles and slug flow is obtained.

<sup>17</sup> Crawford T.J., Weinberger C.B., & Weisman J., (1985) “Two Phase Flow Patterns and Void Fractions...”

## B-DB transition

Turbulent forces increase as the liquid flowrate increases. These turbulent fluctuations cause break up of the larger wobble bubbles. As the turbulence increases all the large wobbly bubbles are sheared into small spherical stable bubbles. The turbulence disperses the bubbles uniformly throughout the liquid and dispersed bubble flow is obtained.

## DB-SL transition

The turbulent fluctuations will maintain a uniform distribution of the small stable bubbles. They can however only be packed to a maximum allowable value. Above this value coalescence is inevitable and the bubbles will collide and form large Taylor bubbles.

## SL-C transition

The transition from slug to churn is of severe complexity and the mechanism is not fully understood. Different theories are presented, but based on different approaches. Nicklin & Davidson<sup>18</sup> suggested that the transition occurs when the velocity of the downward flowing liquid film relative to the velocity of the upward flowing Taylor bubble approaches flooding conditions. Griffith & Wallis<sup>19</sup> suggested that the transition occurs when the Taylor bubble becomes very long. Taitel et al<sup>15</sup> suggested that Churn flow is an entry phenomenon and that stable slug flow will be obtained after a certain entry length.

## A.1.5 Inclined Pipes – Flow patterns

Flow patterns in inclined pipes adopt the same flow regimes as for horizontal and vertical flow. However, certain regimes exist only in certain inclination intervals. Flow pattern maps for near horizontal flow display similarities to the horizontal flow maps. As the angle increases (upward inclined) similarities to upward vertical flow are found. As the angle decreases from horizontal (downward inclined) similarities to downward vertical flow can be found. Inclined flow patterns are complicated because at lower inclinations they will have mechanisms similar to horizontal flow while at steeper inclinations they become similar to vertical. Barnea<sup>20</sup> presented a model where the dominant mechanism is determined for the whole range of inclinations and thereby the transition zones. The transition zones are illustrated in figure 11.23 and 11.24.

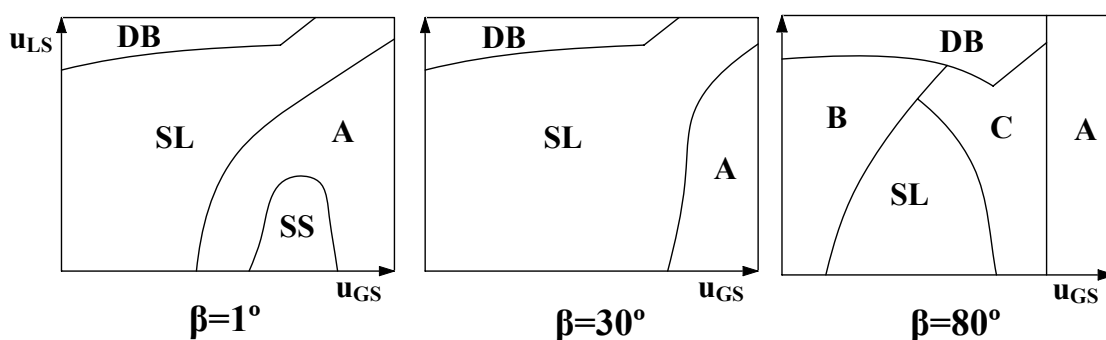


Figure 11.23. Flow pattern maps for three upward inclinations.  $\beta$  is the angle to horizontal.

<sup>18</sup> Nicklin D. J. and Davidson J. F. (1962), "The Onset of Instability on Two Phase Slug Flow."

<sup>19</sup> Griffith P. and Wallis G.B.(1961), "Two Phase Slug Flow"

<sup>20</sup> Barnea D.(1987), "A Unified Model for Predicting Flow Pattern Transitions for the Whole Range of Pipe..."

## Appendix A

If figure 11.23 is compared to the horizontal and upward vertical flow pattern map figure 11.1 and 11.13 it is noticed that the variation near horizontal is great while the variation near vertical is modest.

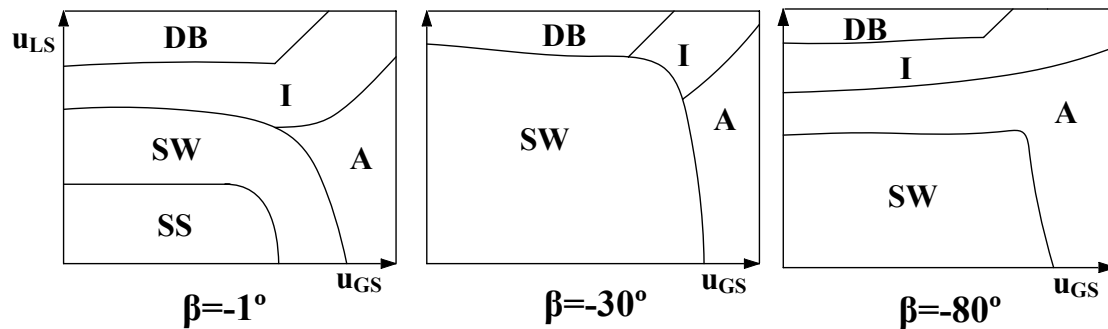


Figure 11.24. Flow pattern maps for three upward inclinations.  $\beta$  is the angle to horizontal.

The flow regimes which generally can be obtained for vertical flow is described in the following.

### Stratified flow

The stratified flow is as for horizontal flow a regime where the phases flow segregated. The liquid flows in the bottom of the pipe and the gas flows above. The gas will normally flow at a higher velocity than the liquid. The liquid can achieve a higher velocity, at certain inclinations and flowrates due to gravity, which affects the interfacial shear between the phases.

At upward inclined flow the liquid velocity will decrease causing a higher liquid height in the pipe. For downward inclined pipes the liquid velocity will increase causing a lower liquid height.

### Intermittent flow

Intermittent flow refers to slug flow and churn flow. Churn flow is not obtainable at lower inclinations. The wobbly bubbles will migrate to the upper pipe wall where coalescence will occur and result in slug flow. The velocity of the film sheered from the liquid slug will at an upward angle change direction and will start to flow downwards.

### Dispersed bubble flow

The dispersed bubble flow regime is similar to the horizontal regime, due to the fact that the turbulent fluctuations are dominant and buoyant forces are neglectable.

### Annular flow

Annular flow refers to the distribution where a high-velocity gas core with entrained liquid drops is encircled by a liquid film at the pipe wall. This regime occurs only at high liquid rates, except for downward near vertical flow. There are no entrained droplets in the gas core in the low gas velocity regime and it is also often denoted Falling Film.

### A.1.6 Inclined Pipes – Transitions

The triggering mechanism which takes place at the transition zone is difficult to categorize for inclined pipes. This is because the dominant mechanism varies with the inclination. Certain mechanism may become inoperative at certain inclination and other mechanism may be dominated by a different mechanism.